

Populating the Black Hole Mass Gaps In Stellar Clusters: General Relations and Upper Limits

JOHAN SAMSING ¹ AND KENTA HOTOKEZAKA^{2,3}

¹*Niels Bohr International Academy, The Niels Bohr Institute,
Blegdamsvej 17, 2100 Copenhagen, Denmark.*

²*Department of Astrophysical Sciences, Princeton University,
Peyton Hall, 4 Ivy Lane, Princeton, NJ 08544, USA.*

³*Research Center for the Early Universe, Graduate School of Science,
University of Tokyo, Bunkyo-ku, Tokyo 113-0033, Japan.*

Submitted to ApJ

ABSTRACT

Theory and observations suggest that single-star evolution is not able to produce black holes (BHs) with masses in the range $3 - 5M_{\odot}$ and above $\sim 45M_{\odot}$, referred to as the lower mass gap (LMG) and the upper mass gap (UMG), respectively. However, it is possible to form BHs in these gaps through merger of compact objects in dense clusters, e.g. the LMG and the UMG can be populated through binary neutron star- and BBH mergers, respectively. This implies that if binary mergers are observed in gravitational waves (GWs) with at least one mass gap object, then either clusters are effective in assembling binary mergers, or our single-star models have to be revised. Understanding how effective clusters are at populating both mass gaps have therefore major implications for both stellar- and GW astrophysics. In this paper we present a systematic study on how efficient stellar clusters are at populating both mass gaps through in-cluster GW mergers. For this, we derive a set of closed form relations for describing the evolution of compact object binaries undergoing dynamical interactions and GW merger inside their cluster. By considering both static and time evolving populations, we find in particular that globular clusters are clearly inefficient at populating the LMG in contrast to the UMG. We further describe how these results relate to the characteristic mass, time, and length scales associated with the problem.

Keywords: gravitational waves, neutron stars, black holes, black hole mass gaps, stellar dynamics

1. INTRODUCTION

Several gravitational wave (GW) sources have now been observed by the LIGO and Virgo GW observatories, including both binary black holes (BBHs) (Abbott et al. 2016a,b,c, 2017a,b; Zackay et al. 2019; Venumadhav et al. 2019), and binary neutron stars (BNSs) (Abbott et al. 2017c). Their astrophysical origin is still unknown, but several formation channels have been suggested. Some of the recently proposed include: field binaries (Dominik et al. 2012, 2013, 2015; Kimugawa et al. 2014; Belczynski et al. 2016b,a; Silsbee & Tremaine

2017; Murguia-Berthier et al. 2017; Rodriguez & Antonini 2018; Schröder et al. 2018), dense stellar clusters (Portegies Zwart & McMillan 2000; Banerjee et al. 2010; Tanikawa 2013; Bae et al. 2014; Rodriguez et al. 2015, 2016a,b,b; Askar et al. 2017; Park et al. 2017; Samsing 2018; Samsing & D’Orazio 2018; Samsing et al. 2019a), active galactic nuclei (AGN) discs (Bartos et al. 2017; Stone et al. 2017; McKernan et al. 2017; Tagawa et al. 2019), galactic nuclei (GN) (O’Leary et al. 2009; Hong & Lee 2015; VanLandingham et al. 2016; Antonini & Rasio 2016; Stephan et al. 2016; Hoang et al. 2017; Hamers et al. 2018), very massive stellar mergers (Loeb 2016; Woosley 2016; Janiuk et al. 2017; D’Orazio & Loeb 2017), and single-single GW captures of primordial black holes (Bird et al. 2016; Cholis et al. 2016; Sasaki et al. 2016; Carr et al. 2016).

The question is, which of these proposed merger channels dominate the merger rate? Are several channels operating with a possible dependence on redshift? Or are the majority of GW sources formed through a still unknown mechanism? Several studies show that one can distinguish at least classes of channels apart, such as isolated binaries and dynamically induced mergers, by considering the observed distribution of merger masses (Zevin et al. 2017), the relative spin orientation of the merging objects (Rodriguez et al. 2016c), as well as the orbital eccentricity at some reference GW frequency (Gültekin et al. 2006; Samsing et al. 2014; Samsing & Ramirez-Ruiz 2017; Samsing & Ilan 2018; Samsing et al. 2018b; Samsing 2018; Samsing et al. 2018a; Samsing & D’Orazio 2018; Rodriguez et al. 2018; Zevin et al. 2019; Samsing et al. 2019b,a). Other ‘indirect’ probes have also been suggested, such as stellar tidal disruptions (e.g. Samsing et al. 2019c; Lopez et al. 2019; Kremer et al. 2019a). In this picture, it is now largely believed that dynamically assembled mergers are likely to have mass ratios near one (e.g. Rodriguez et al. 2018), random relative spin orientations (e.g. Rodriguez et al. 2016c), and a non-negligible fraction of mergers with measurable eccentricity in both LISA (Samsing & D’Orazio 2018; Kremer et al. 2019b), DECIGO/Tian-Qin (e.g. Chen & Amaro-Seoane 2017; Samsing et al. 2019a), and LIGO (Samsing 2018). This is in contrast to isolated binary mergers, that likely have correlated spins (e.g. Kalogera 2000), a bimodal distribution for the effective spin parameter (Zaldarriaga et al. 2018; Hotokezaka & Piran 2017; Piran & Piran 2020), larger mass ratios, and merge on orbits with eccentricities indistinguishable from ≈ 0 near LISA and LIGO. This picture is rather clean when comparing mergers forming in highly dynamical systems, such as globular clusters (GCs) and GN, to completely isolated field binary mergers; however, it becomes less clean when considering e.g. the proposed sub-population of field binaries that undergo secular interactions with nearby single or binary objects (e.g. Naoz et al. 2013; Naoz 2016; Toonen et al. 2016; Antonini et al. 2017; Silsbee & Tremaine 2017; Liu & Lai 2018; Rodriguez & Antonini 2018; Randall & Xianyu 2018a; Antonini et al. 2018; Liu & Lai 2019; Fragione & Loeb 2019; Fragione & Kocsis 2019; Hamers & Thompson 2019; Safarzadeh et al. 2020). In this case, secular exchanges of especially angular momentum, can drive the binary to merge with random spin orientations (e.g. Liu & Lai 2017), and notable eccentricity (e.g. Randall & Xianyu 2018b; Liu et al. 2019; Fragione & Kocsis 2020), which makes it more challenging to disentangle cluster mergers from field binary mergers.

An additional outcome that is somewhat unique to dynamically environments is the formation of so-called hierarchical mergers (e.g. O’Leary et al. 2016; Fishbach et al. 2017; Gerosa & Berti 2017; Yang et al. 2019; Antonini et al. 2019; Gerosa & Berti 2019; Samsing & Ilan 2019; Rodriguez et al. 2019; Gerosa et al. 2020; Safarzadeh et al. 2020; Gayathri et al. 2020; Kimball et al. 2020; Doctor et al. 2020; Baibhav et al. 2020). The picture is here that compact objects (COs) that merge inside their cluster through e.g. single-single GW captures (e.g. Samsing et al. 2019a) or through chaotic few-body interactions (e.g. Samsing et al. 2014; Zevin et al. 2019), will form a new population of ‘second-generation’ (2G) objects that are characterized by having a higher mass than the original ‘first-generation’ (1G) population, and a dimensional spin parameter around 0.7 (e.g. Berti et al. 2007). This 2G population can undergo further interactions leading to merger with other 1G or 2G objects, which then naturally will lead to an observable modified BBH mass spectrum, and spin distribution. This process can in principle also lead to 3G-, 4G-, ..., NG -populations, which naturally gives rise to unique observables. Looking for such hierarchical merger configurations has been proposed to be one way of probing the origin of GW mergers in very dense systems, such as GCs (Rodriguez et al. 2019), GN (Antonini & Rasio 2016), and AGN disks (Yang et al. 2019). However, fine-tuned few-body configurations in the binary field population can in principle also create hierarchical mergers (e.g. Safarzadeh et al. 2020), but in this case it is highly unlikely to go beyond 2G. In any case, an observation of a hierarchical merger would strongly indicate that at least some GW sources are assembled as a result of few-body interactions.

Another interesting consequence of the hierarchical merger scenario is the possibility of populating the so-called lower mass gap (LMG) and upper mass gap (UMG), where the LMG is $\sim 3M_{\odot} - 5M_{\odot}$ (Bailyn et al. 1998; Özel et al. 2010; Farr et al. 2011) and the UMG is marked by a lower limit of $\sim 45M_{\odot}$ (Woosley 2017; Leung et al. 2019; Farmer et al. 2019). For example, the LMG might be populated through BNS collisions, where the UMG can be populated by BBH mergers. This makes it possible for dense clusters to produce GW sources with objects in either the LMG or the UMG. If ‘Nature’ is not able to form BHs through single star evolution in these mass gaps, then an observation of GW sources with a mass-gap object will give us insight into the fraction of mergers assembled in clusters, or at least dynamically. These mass-gaps not only play a key role in stellar-astrophysics, but introduce also a character-

istic mass scale that can be used to e.g. constrain the cosmological parameters (Farr et al. 2019).

Several recent studies have discussed the possibility of populating the mass-gap in clusters (e.g. Rodriguez et al. 2019; Doctor et al. 2020; Baibhav et al. 2020). Currently, numerical studies suggest that BNS mergers are not likely to form in systems such as GCs (e.g. Ye et al. 2020). On the other hand, recent observations of the orbital parameters of galactic BNSs interestingly indicate that BNSs might actually form in clusters at rates several orders-of-magnitude higher than suggested by the numerical studies (e.g. Andrews & Mandel 2019), which of course poses some interesting tension. Regarding BBHs, several studies have found that if the initial BH spins are low, then up to $\sim 10\%$ of BBH mergers from GCs could be in the form of 1G-2G binaries, with a sub-fraction of these being in the UMG (Rodriguez et al. 2019). To find the observable contribution from such hierarchical mergers in upcoming and future GW data several numerical techniques and models are now under development (e.g. Doctor et al. 2020); however, common for the majority of these models is that they are not linked to any real physical model, they are instead just generic functional forms with a few fitting parameters. This kind of model independent approach might be useful to condense a huge stream of data into just a few fitting parameters, but gives a-priori no astrophysical insight into what systems that are likely and able to undergo hierarchical mergers and populating the mass-gaps.

In this paper we derive a set of fundamental relations describing how effective a dense cluster can grow a 2G-population from a series of in-cluster GW mergers of 1G-1G binaries, as a function of characteristic mass, length, and time scales of the 1G objects and their cluster. The core of our calculations are based on the post-Newtonian (PN) binary-single hardening model presented in Samsing (2018); Samsing & D’Orazio (2018), where binaries are able to merge in-between or during their hard binary-single interactions. We use our derived expressions to make general statements about what clusters that are able to populate the LMG through BNS mergers, and the UMG through BBH mergers. Our model is fully analytical and our results are given in closed form expressions, and as a result, we are therefore only able to describe idealized clusters with constant density and velocity dispersion (for an extension of our model see e.g. Antonini & Gieles 2020); however, our work serves as an important first step in connecting physical parameters with more general statements related to hierarchical mergers (see also recent work by Baibhav et al. 2020).

The paper is organized as follows. In Sec. 2 we introduce our dynamical cluster- and 3-body interaction model, and use it to derive results on how efficient a simple non-evolving binary and single cluster population is at producing in-cluster GW mergers. In Sec. 3 we extend our model to include a time dependent distribution of both singles and binaries, from which we derive a closed form solution to the upper limit on the number of 2G-objects relative to 1G-objects a given cluster can reach in a Hubble time. We further discuss these results in relation to populating the LMG and the UMG. We conclude our study in Sec. 4.

2. FORMATION OF IN-CLUSTER MERGERS

We consider a cluster with a population of COs (NSs or BHs), each with a mass m . These COs interact, and can through different dynamical pathways merge through the emission of GWs either inside or outside of their cluster (e.g. Samsing & D’Orazio 2018; Rodriguez et al. 2018). The COs that merge inside the cluster give rise to a growing in-cluster population of BHs with a mass $\approx 2m$, given that the kick velocity associated with asymmetric GW emission at merger is smaller than the cluster escape velocity (e.g. Gerosa & Berti 2019). In this work we refer to the initial population of COs by ‘1’ or 1. generation (1G) objects, and the population of BHs that is formed through the collision of 1G-1G binaries by ‘2’, or 2. generation (2G). As described in the Introduction, the 2G population is able to populate both the lower ($3 - 5M_\odot$) and upper ($> 45M_\odot$) BH mass gaps that are believed to be associated with the initial 1G population. For example, it might be possible to populate the $3 - 5M_\odot$ BH mass-gap through the collision of BNSs.

Below we start by deriving and present a set of basic relations for describing the growth of 2G populations through in-cluster 1G-1G GW mergers. Throughout the paper we mainly illustrate results for our two fiducial mass cases; $m = 1.4M_\odot$ and $m = 30M_\odot$, which are in the relevant range for populating the LMG and the UMG, respectively.

2.1. Cluster Model and 3-Body Dynamics

In this work we study a model described by a cluster consisting of COs all with the same mass m . The cluster itself is assumed to have a constant number density of singles n , velocity dispersion v_d , and escape velocity $v_e = f_{ed} \times v_d$. Besides this single population, the cluster also harbors a population of CO binaries, that at early times consist of 1G-1G pairs, but at later times, through dynamical exchange interactions, can evolve to have pairs also including 2G objects. The binaries play

a very important role, as these provide the main pathway for producing 2G-objects as a result of binary-single interactions. In-cluster GW mergers can also form in other ways, such as through single-single GW captures (Samsing et al. 2019a), secular Kozai triples (Antonini et al. 2016), and binary-binary interactions (Zevin et al. 2019); however, these pathways are generally subdominant compared to the binary-single channel. Our main discussions will therefore mostly involve mergers from the interacting binary-single population. In the sections below we continue by describing the basics of our cluster model.

2.1.1. Binary Hardening and Outcomes

We assume that a given CO binary inside the cluster forms (dynamically) with a semi-major (SMA), a , equal to the hard-binary (HB) limit value (e.g. Heggie 1975; Aarseth & Heggie 1976; Hut & Bahcall 1983),

$$a_{HB} = \frac{3G}{2} \times \frac{m}{v_d^2}, \quad (1)$$

which is where the binary binding energy ($Gm^2/(2a)$) equals the kinetic energy of the surrounding singles w.r.t. the binary ($mv_d^2/3$). After this, the binary undergoes scatterings with the surrounding singles, each of which leads to a decrease in the SMA of the binary from a to δa . This corresponds to a change in a of $-a(1-\delta) = -a\Delta$, where we have introduced $\Delta \equiv 1-\delta$ to shorten notations. In reality, the change per interaction in the binary binding energy E_b follows approximately a power-law distribution $P(E_b) \propto E_b^{-\gamma}$ with $\gamma \sim 9/2$, depending on exactly how a strong binary-single interaction is defined (e.g. Heggie 1975; Stone & Leigh 2019). In this work we do not use the full distribution, instead we assume that each interaction leads to a fixed fractional decrease δ in the SMA, that is equal to the average value found from the distribution $P(E_b) \propto E_b^{-\gamma}$. Using that $E_b = -Gm^2/(2a)$, and that $\delta \equiv \langle a \rangle / a_0$, where a_0 is the initial SMA and $\langle a \rangle$ is the average value of the resulting SMA, then δ is given by (see also Samsing 2018),

$$\begin{aligned} \delta &= (\gamma - 1) \int_0^1 \delta^{(\gamma-1)} d\delta = 1 - \gamma^{-1}, \\ &= 7/9, \quad (\gamma = 9/2). \end{aligned} \quad (2)$$

The binary keeps undergoing these so-called ‘hardening’ interactions with the surrounding single population, until its SMA reaches one of the following three characteristic values: The first, denoted by a_{ej} , is the maximum SMA value for which the binary will get ejected out of the cluster if it undergoes a binary-single interaction. Note that this is a fixed value in our simple ‘ δ -model’.

The second, denoted by a_{GW} , is the SMA for which the total integrated probability for the binary to merge at any given state from a_{HB} to a_{GW} equals one. The merging binary will of course have a decreasing SMA as it inspirals, but will during this time not interact with other objects. The third, denoted by a_{tH} , is the value it takes a Hubble time to reach through binary-single interactions alone from the initial value a_{HB} . The hierarchy of these three characteristic scales is set by (v_d, n, m) , and plays a key role in how to grow a 2G BH population inside the cluster through in-cluster mergers (see also Antonini & Rasio 2016; Antonini & Gieles 2020; Baibhav et al. 2020). For example, if $a_{ej} > a_{GW}$ then most binaries will get ejected and merge outside of the cluster, compared to if $a_{GW} > a_{ej}$ in which case all binaries will merge inside. If on the other hand $a_{tH} > \{a_{ej}, a_{GW}\}$ then the system will not be able to conclude even a single interaction sequence, and an effective accumulation of 2G mergers is therefore near impossible. As a result, the ‘relevant’ value for a given system is

$$a_m = \max(\{a_{ej}, a_{GW}, a_{tH}\}), \quad (3)$$

where the sub-script ‘ m ’ here refers to ‘minimum’, as this is the smallest value the SMA of the interacting binary can take. This δ -model is further illustrated and described in Fig. 1.

Throughout the paper we refer to the process in which the system brings a binary from a_{HB} to a_m through binary-single interactions alone as one ‘Interaction Cycle’ (IC). After a binary has completed its IC, then it generally happens that a new binary dynamically forms with a SMA $\sim a_{HB}$, after which the process repeats. This cycle of binary formation and hardening interactions is also often referred to as ‘binary burning’ (e.g. Kremer et al. 2020). We continue below by deriving a_{ej} , a_{GW} , and a_{tH} . We also refer the reader to (Antonini & Rasio 2016; Antonini & Gieles 2020; Baibhav et al. 2020) for complementary discussions on this.

2.1.2. Derivation of Outcome Conditions

For calculating the SMA at which the binary is ejected, a_{ej} , we first use that the energy released in one interaction between a single and a binary with SMA a is given by $E_{bs} = (\Delta/\delta) \times E_b(a)$, where $E_b(a)$ is the internal energy of the binary before interaction (e.g. Samsing 2018). The energy E_{bs} is ‘released’ in the three-body center-of-mass (COM), which in the Newtonian limit is conserved from before to after the interaction. From momentum conservation it then follows that the binary receives a velocity kick, defined at infinity in the COM, of $v_b^2 = E_{bs}/(3m) = (1/6)(\Delta/\delta)Gm/a$. When a is such that $v_b > v_e$ then the binary escapes the cluster. By

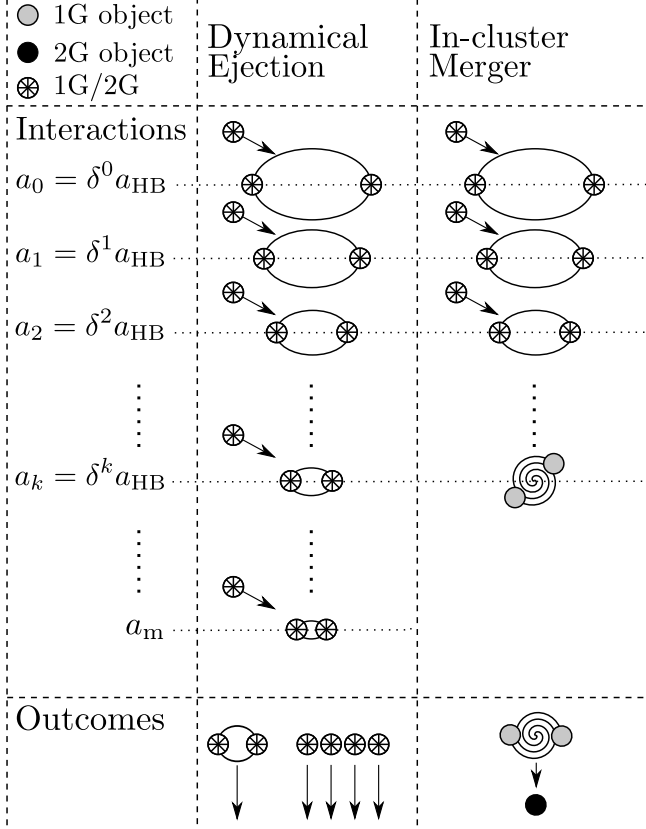


Figure 1. Illustration of our δ -model described in Sec. 2.1. In this model we assume that all binaries dynamically form at the HB-limit inside the cluster, after which they undergo scatterings with the surrounding singles. Each scattering leads to a fixed decrease in the SMA from a to δa , as shown in the left column (*Interactions*). This series of hardening interactions terminate at a characteristic SMA a_m , that either is where the binary merges inside the cluster, is being ejected, or when the time passes t_H , as further described in Sec. 2.1.1. The middle and the right columns show the two scenarios where the binary is either ejected (*Dynamical Ejection*), or merges inside the cluster (*In-cluster Merger*), respectively. The outcome from each of these scenarios is shown in the bottom panel (*Outcomes*). As seen, the outcome from a dynamical ejection is 1 binary and ~ 4 singles, where for 1G-1G in-cluster mergers the outcome is per definition a 2G-object. When following the in-cluster population of 1G and 2G objects over time, the *Dynamical Ejection* outcome always acts as a ‘sink term’, where the 1G-1G *In-cluster Merger* outcome is the ‘source term’ for the 2G population, as further described in Sec. 3.1. Note that the *grey* and *black* circles refer to 1G- and 2G-objects, respectively, where the *diamond* symbol denotes either of these two objects.

now defining $a_{ej} \equiv a(v_b = v_e)$ it then follows that,

$$a_{ej} \approx \frac{G\Delta}{6\delta f_{ed}^2} \times \frac{m}{v_d^2}. \quad (4)$$

Note here that $a_{HB}/a_{ej} = 9f_{ed}^2\delta/\Delta = (63/2)f_{ed}^2$, where we have set $\delta = 7/9$ in the last equality. A single bi-

nary therefore has to decrease its SMA by 1-2 orders of magnitude through binary-single scatterings before a possible ejection can take place. As will be discussed and used later, several of the single objects interacting with the binary will also get ejected, as they likewise receive recoil kicks during the hardening process. As a result, for every single binary ejected there will also be N_s^{ej} single objects ejected. This number N_s^{ej} can be estimated by first comparing the SMA below which single ejections are possible, $a_{ej}^s \approx 2G\Delta/(3\delta f_{ed}^2) \times m/v_d^2$, where we have used $2v_b = v_s$, with the binary ejection SMA a_{ej} from Eq. (4). As seen, $a_{ej}^s/a_{ej} = 4$. Now using that after Δn binary-single interactions the binary SMA decreases by a factor $\delta^{\Delta n}$, it then follows that $N_s^{ej} = \ln(1/4)/\ln\delta \approx 5$, where we have used that one single object is ejected in each scattering for $a_{ej} \leq a \leq a_{ej}^s$. The number N_s^{ej} is therefore a constant that does not depend on any properties of the system, as long all the interaction steps are ‘available’. In this paper we use $N_s^{ej} = 4$, as this value is slightly closer to what is found in numerical simulations; however, the exact value does not play a large role, the important point is that it takes a constant value.

For a_{GW} , we start by calculating the probability that a binary with SMA a merges before its next binary-single interaction, denoted here by $p_2(a)$. For this we assume that the eccentricity distribution of the binary follows that of a thermal distribution, $P(e) = 2e$ (e.g. Heggie 1975). In addition, we use that the time in-between binary-single interactions, $t_{bs}(a)$, is the inverse of the binary-single encounter rate, $t_{bs}(a) \approx (n\sigma_{bs}v_d)^{-1}$, where $\sigma_{bs} \propto ma/v_d^2$ is the HB binary-single interaction cross section (see e.g. Samsing et al. 2018b). Under these assumptions it directly follows that $p_2(a) = (t_{bs}(a)/t_{GW}(a))^{2/7}$, where $t_{GW}(a) \propto a^4/m^3$ is the GW inspiral life time corresponding to $e = 0$ (e.g. Samsing 2018). This $p_2(a)$ is only the probability for merger during a single ‘interaction step’ k , where we here introduce the notation $a_k = a_{HB}\delta^k$. The total probability for a binary to merge in-between its binary-single interactions from a_{HB} to a_m , denoted by $P_2(a_m)$, is therefore found by simply integrating from $k(a_{HB}) = 0$ to $k(a_m)$. Using that $da = -a\Delta dk$, the solution is found to be $P_2(a_m) \approx p_2(a_m) \times (7/(10\Delta))$ (e.g. Samsing 2018; Samsing et al. 2019c), which can be written out as,

$$P_2(a_m) \approx A_c^{2/7} \times \frac{m^{4/7}v_d^{2/7}}{n^{2/7}a_m^{10/7}}, \quad (5)$$

where we have assumed that $p_2(a_m) \gg p_2(a_{HB})$ and defined the constant $A_c = (7^{7/2}85G^2)/((10\Delta)^{7/2}9\pi c^5)$. If we now set $P_2 = 1$ then the corresponding $a_{GW} \equiv$

$a(P_2 = 1)$ can now be isolated and gives,

$$a_{GW} = A_c^{1/5} \times \frac{m^{2/5} v_d^{1/5}}{n^{1/5}}. \quad (6)$$

As seen, this limit is surprisingly insensitive to the cluster parameters v_d and n (see also Antonini & Rasio 2016).

The last characteristic SMA we consider is a_{tH} , which is the value for which it takes the binary a Hubble time to reach from $a = a_{HB}$ through binary-single interactions alone. For calculating this, we start with the time it takes the binary to undergo one interaction at interaction step ‘ k ’, which can be approximated as $t_{bs}(a_k) \approx (n\sigma_{bs}(a_k)v_d)^{-1}$ (see the above paragraph). The total time it takes to reach a_m , denoted by τ_m , is found by integration $t_{bs}(a_k)$ from $k(a_{HB}) = 0$ to $k(a_m)$. From this, one finds that $\tau_m \approx t_{bs}(a_m)/\Delta$, which also can be written as,

$$\tau_m \approx (6\pi G \Delta)^{-1} \times \frac{1}{a_m} \frac{v_d}{nm}, \quad (7)$$

where we have assumed that $a_{HB} \gg a_m$. Setting this expression for τ_m equal to t_H , and isolating the corresponding $a_{tH} \equiv a_m(\tau_m = t_H)$, one now finds,

$$a_{tH} \approx \frac{(6\pi G \Delta)^{-1}}{t_H} \times \frac{v_d}{nm}, \quad (8)$$

which relates to a_{HB} as $a_{HB}/a_{tH} \approx (t_H/t_{bs}(a_{HB}))\Delta$.

2.2. Results

Having derived analytical expressions for the three characteristic scales a_{ej} , a_{GW} , and a_{tH} in Sec. 2.1.2 above, we are now in a position to start exploring what cluster systems that are likely to grow a population of 2G objects. In the sections below we study this by considering a few general relations and overview figures for a ‘static’ cluster population. In Sec. 3 we use these results to model ‘time evolving’ populations.

2.2.1. Outcome Regions

Fig. 2 shows $a_m = \max(\{a_{ej}, a_{GW}, a_{tH}\})$ with colored regions (blue, red, grey) as a function of cluster velocity dispersion v_d and number density n for $m = 30M_\odot$ (top) and $m = 1.4M_\odot$ (bottom). The three regions are separated by green dashed lines, where the point at which all of the three regions meet, a point we refer to the ‘break point’ (BP), is highlighted with a green circular dot. How the green dashed lines depend on the parameters v_d, n, m , provide the key to understand what systems that are likely to produce a sizable population of 2G objects. Below we study this in more detail. Our

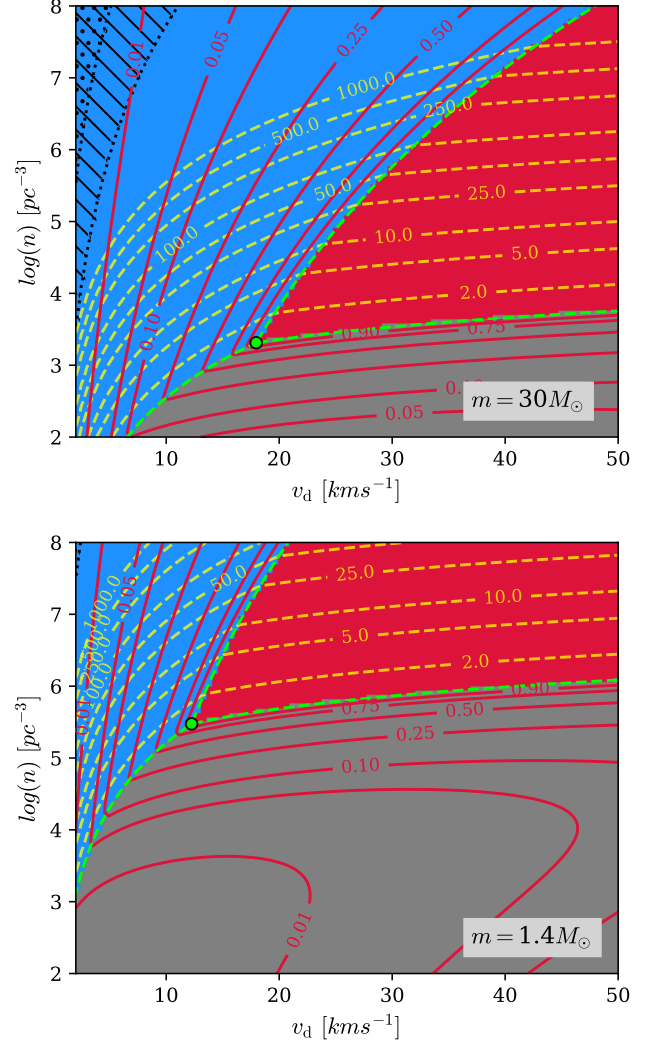


Figure 2. Results for a binary interacting with singles in a cluster described by a velocity dispersion $v_d = v_e/\sqrt{12}$, and number density n . The objects all have the same mass m , where $m = 30M_\odot$ (BH) and $m = 1.4M_\odot$ (NS) in the *top plot* and the *bottom plot*, respectively. The binary evolution is modeled using our δ -model described in Sec. 2.1. In this model, the IC outcome of a given binary will fall into one of the following three general categories: (1) *Blue region*: The binary can get ejected through a binary-single interaction ($a_m = a_{ej}$). (2) *Red region*: The binary will always merge inside the cluster before ejection is possible ($a_m = a_{GW}$). (3) *Grey region*: The binary will not be able to finish a single IC within a Hubble time ($a_m = a_{tH}$). The green dashed lines separating these outcome regions are discussed in Sec. 2.2.1. The red solid lines show the total probability for a binary to merge inside the cluster during one IC, $P_M = P_2 + P_3$, where the orange dashed lines show the number of ICs a binary can undergo in Hubble time, $N_c(t_H)$. The hatched region shows where $P_3 > P_2$, where the dotted region shows where $\Gamma_{ss} > \Gamma_{23}$ for $N_b/N_s = 0.05$, as further described in Sec. 2.2.2.

expressions are written out for $\delta = 7/9$ if nothing else is stated.

We start by the line separating the two regions a_{ej} (blue) and a_{tH} (grey) to the left of the BP. By now setting $a_{ej} = a_{tH}$ and solving for the corresponding $n(ej, tH) \equiv n(a_{ej} = a_{tH})$ one finds,

$$n(ej, tH) = \left[\frac{63}{4\pi} \frac{f_{ed}^2}{G^2 t_H} \right] \times \frac{v_d^3}{m^2}, \quad (9)$$

where we used Eq. (4) and (8). The next line is the one separating the regions a_{ej} (blue) and a_{GW} (red) to the right of the BP. Following the same procedure as above, we first set $a_{ej} = a_{GW}$ and solve for the corresponding $n(ej, GW)$,

$$n(ej, GW) = \left[\frac{1}{B_c} \frac{f_{ed}^{10}}{G^3 c^5} \right] \times \frac{v_d^{11}}{m^3}, \quad (10)$$

where we have used Eq. (4) and (6), and introduced the constant $B_c = (9\pi/(21^{5/85}))(20/63)^{7/2}$. Finally, the line separating a_{GW} (red) and a_{tH} (grey) to the right of the BP is found from setting $a_{GW} = a_{tH}$, from which we find,

$$n(GW, tH) = \left[\left(\frac{63}{4\pi} \right)^5 \frac{B_c c^5}{G^7 t_H^5} \right]^{1/4} \times \frac{v_d}{m^{7/4}}, \quad (11)$$

where we have used Eq. (6) and (8). The associated coordinates of the BP, denoted by $(v_d(BP), n(BP))$, can now be found from, e.g., setting $n(ej, tH) = n(ej, GW)$ from which follows,

$$v_d(BP) = \left[\frac{63}{4\pi} \frac{B_c G c^5}{f_{ed}^8 t_H} \right]^{1/8} \times m^{1/8},$$

$$n(BP) = \left[\left(\frac{63}{4\pi} \right)^{11} \frac{B_c^3 c^{15}}{G^{13} f_{ed}^8 t_H^{11}} \right]^{1/8} \times m^{-13/8}. \quad (12)$$

As seen here, the BP coordinates $v_d(BP), n(BP)$ are $\propto m^{1/8}, m^{-13/8}$, respectively. Therefore, the location of the BP along the v_d -axis remains almost constant for reasonable changes in m , in contrast to the location along the n -axis, which can change by orders-of-magnitude. As a result, for 1G objects in the mass range $1M_\odot \lesssim m \lesssim 50M_\odot$ the BP will always be around $10 \sim 20 \text{ km s}^{-1}$, which is slightly higher than the dispersion velocity of a typical GC. Since no configurations with $a_m = a_{GW}$ are possible for values of $v_d < v_d(BP)$ it then follows that GCs will in theory never be able produce binaries that only have the option of merging inside the cluster. The relevant value of a_m for GCs is then either a_{ej} or a_{tH} . This of course could also be used to argue why GCs have the properties they do, such

as long time stability and no (visible) central massive BHs. Indeed, several studies have shown that velocity dispersion do act as central parameter for distinguishing e.g. GCs from NSCs with massive central BHs (e.g. Miller & Davies 2012; Antonini & Rasio 2016). If some GCs have massive BHs in the range of $10^3 - 10^4 M_\odot$ in their center is still the focus of both observational (e.g. Kızıltan et al. 2017) and theoretical work (e.g. Gültekin et al. 2004; Giersz et al. 2015; Fragione & Bromberg 2019; Hénault-Brunet et al. 2020), and could provide insight into the formation of the super-massive BHs seen in most galactic centre (e.g. Miller & Davies 2012; Antonini et al. 2019). Another feature linked to the BP is that clusters with $n \gtrsim n(BP)$ will (nearly) always produce and process binaries that undergo at least one IC due to the relative weak dependence on v_d for the $n(GW, tH)$ -boundary. Regarding the dependence on m , one sees that the boundary quickly moves up for decreasing values of m , as $n(BP) \propto m^{-13/8}$. This makes it increasingly difficult for 1G-objects with masses in the range $m \sim 1M_\odot$ to undergo more than 1 IC within a Hubble time for astrophysical cluster values compared to $m \sim 30M_\odot$ 1G-objects, as clearly seen in Fig. 2. Before we study this in greater detail, we proceed below by exploring to which degree 3-body mergers and single-single (S-S) GW captures contribute to the in-cluster merger rate.

2.2.2. 3-body Mergers and Single-Single GW Captures

Before moving on to how efficient a population of binaries is at producing a 2G population, we here address the potential importance of including the in-cluster merger contribution from S-S GW captures and 3-body mergers. As described in Sec. 2.1, ‘S-S GW captures’ denote the process in which two initially unbound COs become bound through the emission of GWs (e.g. Samsing et al. 2019a), where a ‘3-body merger’ refers to COs merging during a chaotic 3-body interaction (Samsing et al. 2014).

We start by analyzing the contribution from 3-body mergers. For this, we first estimate what part of the (v_d, n) -space the total integrated probability for producing a 3-body merger, P_3 , is larger than the total probability for undergoing a 2-body merger, P_2 . Following Samsing (2018), the probability for a binary-single interaction to produce a 3-body merger can be approximated by $p_3(a) \approx 2\mathcal{N}(\mathcal{R}_m/a)^{5/7}$, where $\mathcal{N} \approx 20$ denotes the number of ‘temporary binary states’ the chaotic triple interaction on average assembles during one interaction, \mathcal{R}_m is the Schwarzschild radius of a BH with mass m , and a is the SMA of the initial target binary. The total probability for a 3-body merger to form during one IC

can now be found from integrating $p_3(a)$ from $a = a_{HB}$ to $a = a_m$, in the same way as we did for finding P_2 in Sec. 2.1.2. Following this approach, one finds that $P_3(a_m) \approx p_3(a_m) \times (7/(5\Delta))$, which can be written out in the following way,

$$P_3(a_m) \approx \left[\frac{2^{12/7} 7}{5\Delta} \frac{\mathcal{N} G^{5/7}}{c^{10/7}} \right] \times m^{5/7} a_m^{-5/7}, \quad (13)$$

where we have assumed that $p_3(a_m) \gg p_3(a_{HB})$ (Note here that we calculate these merger probabilities separately, i.e., we do not take into account the potential interplay between merger channels, including the S-S GW capture channel). From this we see that $P_3(a_m)/P_2(a_m) \propto (n/v_d)^{2/7}$. This indicates that 3-body mergers will provide the greatest contribution relative to the 2-body mergers at high n and low v_d , which is the regime where $a_m = a_{ej}$, as seen on Fig. 2. We therefore need to evaluate and compare P_2 and P_3 for $a_m = a_{ej}$. Using Eq. (5), Eq. (13), and Eq. (4), this first lead us to,

$$P_2(a_{ej}) \approx \left[\frac{1}{B_c} \frac{f_{ed}^{10}}{G^3 c^5} \right]^{2/7} \times \frac{v_d^{22/7}}{m^{6/7} n^{2/7}} \quad (14)$$

and

$$P_3(a_{ej}) \approx \left[\frac{42^{5/7}}{(5/63)} \frac{\mathcal{N} f_{ed}^{10/7}}{c^{10/7}} \right] \times v_d^{10/7}. \quad (15)$$

Now setting these two expressions equal to each other one finds,

$$n(P_2, P_3) \approx \left[\frac{(5/63)^{7/2} f_{ed}^5}{42^{5/2} \mathcal{N}^{7/2} B_c G^3} \right] \times \frac{v_d^6}{m^3}, \quad (16)$$

where $n(P_2, P_3)$ therefore represents the boundary in the $a_m = a_{ej}$ region for which $P_2 = P_3$. This boundary is shown in Fig. 2 with the dotted line that encloses the black solid line hatched area. In this area $P_3 > P_2$. As seen, for most systems, especially the one with relative low mass m and moderate density n , 3-body mergers will not dominate the total in-cluster merger probability. We will therefore in our analytical models throughout this paper omit this contribution for simplicity and clarity.

We now move on to the S-S GW capture population. For this its more easy to compare merger rates, Γ , than probabilities. In this case, the total rate of S-S GW capture mergers from a simple ' $n\sigma v$ ' estimate is given by (Samsing et al. 2019a),

$$\Gamma_{ss} \approx \left[\frac{4\pi G^2}{c^{10/7}} \left(\frac{85\pi}{24\sqrt{2}} \right)^{2/7} \right] \times \frac{N_s m^2}{v_d^{18/7}}, \quad (17)$$

where N_s is the total number of single BHs. Note that we have here assumed that all the single BHs, N_s , are

distributed uniformly according to our model of a constant v_d, n ; however, in reality, the single BHs naturally distribute according to some density and velocity profile. As a result, the real GW capture rate is generally smaller than the one presented in the above Eq. (17), as further discussed in Samsing et al. (2019a). Regarding the merger rate from our considered binary-single interactions, one finds that this can be approximated by,

$$\Gamma_{23} \approx \frac{N_b(P_2(a_m) + P_3(a_m))}{\tau_m}, \quad (18)$$

where $P_2 + P_3 \leq 1$ is the total number (probability) of 2-body and 3-body mergers forming during 1 IC, τ_m is the time it takes for undergoing 1 IC (see Eq. (7)), and N_b is the number of CO binaries in the cluster that contributes to the merger rate. We have here included the 3-body mergers, as it turns out that the S-S GW captures only significantly contribute for low v_d and high n , exactly where the 3-body mergers also contribute. This is seen in Fig. 2, where the black dotted line inclosing the black dotted area is where $\Gamma_{ss} = \Gamma_{23}$ for binary fraction $N_b/N_s = 0.05$. The S-S GW captures are therefore not expected to provide a significant contributing in the regions we are interested in.

To conclude, we have here shown and argued that neither the 3-body mergers nor the S-S GW capture mergers contribute significantly to the in-cluster merger rate. We therefore only consider the 2-body merger contribution in the rest of this paper.

2.2.3. Interaction Cycles and In-cluster Mergers

The number of in-cluster GW mergers that can be produced over a Hubble time per 1G-1G binary, here denoted by $N'_M(t_H)$, serves as an approximate measure for how efficient a given cluster is at growing a 2G population. At this stage we approximate this number by the following product,

$$N'_M(t_H) \approx N_c(t_H) \times P_M, \quad (19)$$

where $N_c(t_H) = t_H/\tau_m$ is the number of ICs a cluster can run through in a Hubble time, i.e. the number of binaries the cluster can process in time t_H , and P_M is the probability for an in-cluster GW merger to form during one IC. In Fig. 2 is shown with *orange dashed lines* and *red solid lines* the contours of $N_c(t_H)$ and P_M , respectively, where for P_M we have here included the probability for 3-body mergers, i.e. $P_M = P_2(a_m) + P_3(a_m)$. In short, our procedure for estimating $N_c(t_H)$ and P_M at a given point (v_d, n) , is first to calculate a_m from Eq. (3), after which we use Eq. (7) to find $N_c(t_H) = t_H/\tau_m$, and Eq. (5) and Eq. (13) to find $P_M = P_2(a_m) + P_3(a_m)$.

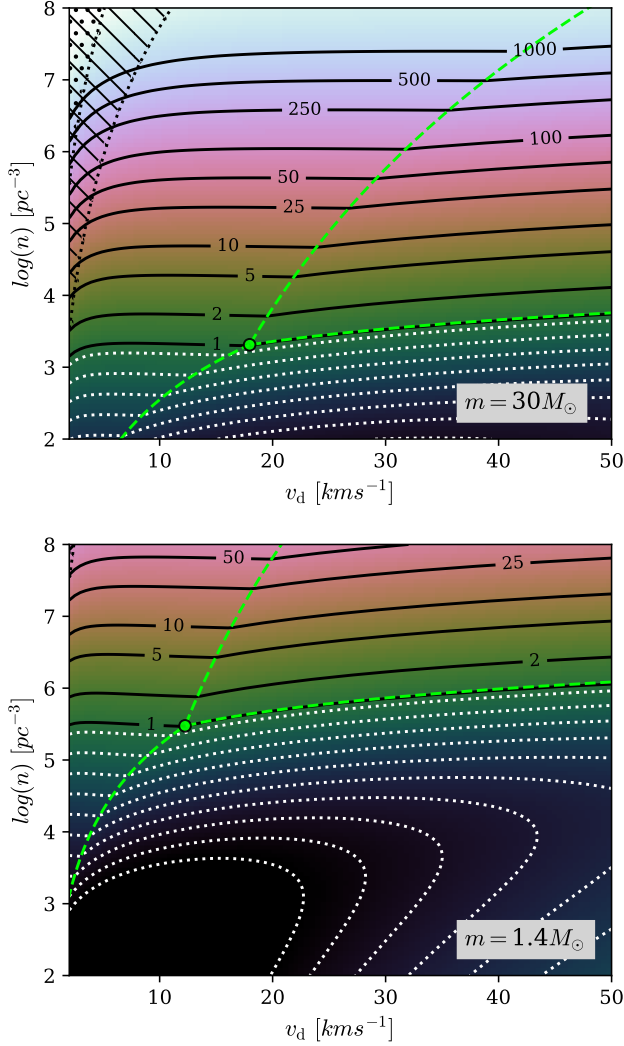


Figure 3. Similar to Fig. 2, but here the *black solid lines* show the corresponding number of in-cluster GW mergers that form in a Hubble time per binary, $N'_M(t_H)$. The *white dotted* contour lines show where $N'_M(t_H) < 1$, and highlights therefore the area for which the system is not effective in growing a 2G population. For this figure we have assumed that $N'_M(t_H) \approx N_c(t_H) \times P_M$, where $N_c(t_H)$ is the number of ICs a binary can undergo in a Hubble time, and $P_M = P_2 + P_3$ is the probability for a binary to undergo an in-cluster GW merger during one IC. These two quantities are also shown separately in Fig. 2. As seen in the figure above, the number $N'_M(t_H)$ is almost independent of v_d , but highly sensitive to especially m .

As seen in Fig. 2, for decreasing values of v_d the probability P_M decreases, which also follows from Eq. (14) where $P_2 \propto v_d^{22/7}$, in contrast to the number of ICs, $N_c(t_H)$, that instead increases. Therefore, one can easily have a cluster with binaries where burning is efficient, i.e. where $N_c(t_H) \gg 1$, but at the same time with a probability for merging during individual ICs is low,

i.e. with $P_M \ll 1$, and vice versa. How these two quantities ‘balance out’ is clear in Fig. 3, which shows in black solid lines $N'_M(t_H)$ from Eq. (19). Surprisingly, the large changes in both P_M and $N_c(t_H)$ as v_d is varied almost cancel out, and $N'_M(t_H)$ is as a result almost flat across v_d . To study this behavior further, we can write out $N'_M(t_H)$ in the region relevant for GC systems where $P_2 \gg P_3$ and $a_m = a_{ej}$ using Eq. (19), Eq. (7) evaluated at $a_m = a_{ej}$, and the expression for $P_2(a_{ej})$ given by Eq. (14), from which one finds,

$$N'_M(t_H) \approx t_H \left[\left(\frac{4\pi}{63} \right)^{7/2} \frac{G^4 f_{ed}^3}{B_c c^5} \right]^{2/7} \times n^{5/7} m^{8/7} v_d^{1/7} \quad (20)$$

$$\approx 0.5 \left(\frac{n}{10^5 \text{ pc}^{-3}} \right)^{5/7} \left(\frac{m}{1.4 M_\odot} \right)^{8/7} \left(\frac{v_d}{10 \text{ km s}^{-1}} \right)^{1/7}, \quad (21)$$

where in the last line we have inserted values relevant for NS-NS mergers. This confirms the results we see in Fig. 3, namely that $N'_M(t_H)$ only depends weakly on v_d as $N'_M(t_H) \propto v_d^{1/7}$. As a result, all systems with $n \gtrsim n(BP)$ will to leading order have $N'_M(t_H) \gtrsim 1$. From this follows that if the number of CO binaries is constant in time at a value N_b , then the number of in-cluster mergers for $n \gtrsim n(BP)$ will be $\gtrsim N_b$ after a Hubble time. For example, for our $m = 30 M_\odot$ case shown in the upper panel of Fig. 3, the number of in-cluster mergers over a Hubble time per binary is of order 10 for $\log n \approx 4 \sim 5 \text{ pc}^{-3}$. If the number of BBHs in the cluster at any given time is a few, say ~ 5 , then our model predicts that the total number of in-cluster mergers forming over a Hubble time is $\sim 5 \times 10 = 50$. Although this number of course fluctuates from cluster to cluster, we note that this number is consistent with what is found using numerical simulations (see Rodriguez et al. (2019), where 48 in-cluster mergers were reported for their example in Sec. IV.A). More generally, $N'_M(t_H)$ provides an upper limit on the number of available 2G objects after a Hubble time produced per cluster binary, as only a small fraction of the in-cluster mergers, i.e. 2G objects, are actually retained by the cluster Rodriguez et al. (2019). The remaining are either kicked out immediately as a result of GW kicks, or later dynamically through e.g. a binary-single interaction. Considering the $m = 1.4 M_\odot$ case, we see both from Eq. (21) and Fig. 3 that $N'_M(t_H)$ is only $\gtrsim 1$ for $\log n \gtrsim 5 - 6 \text{ pc}^{-3}$, which is a very high density threshold for astrophysical standards. This provides a clear hint that clusters hosting only NS-NS binaries are not likely to be effective in turning its population into a sizable

2G population, i.e. in populating the LMG, unless the binary fraction initially is relatively high.

Lastly, in relation to the probability of observing a possible 2G-population from a cluster, what matters is not only the number of 2G-objects produced, but also how many of these that are present in the cluster compared to the number of remaining 1G objects. As described back in Sec. 2.1.2, a single IC will on average give rise to $N_{ej}^s + 2 \sim 6$ ejected 1G-objects (if in-cluster mergers and 2G objects are ignored), which naturally leads to a gradual reduction of this population over time. In our model considered so far, the number of in-cluster GW mergers relative to the number of (remaining) 1G-objects after time t is therefore approximately,

$$\frac{N'_M(t)}{N_1(t)} \approx \frac{N_b N'_M(t)}{N_1(0) - N_b N_c (N_{ej}^s + 2)} \quad (22)$$

$$\approx \frac{N'_M(t)}{f_b^{-1}(0) - N'_{ej}(t)}, \quad (23)$$

where we have assumed that N_b remains constant, $N_1(0)$ denotes the initial number of 1G-objects, $f_b(0) = N_b/N_1(0)$, and $N'_{ej}(t)$ denotes the total number of 1G-objects ejected after time t per binary. We will explore this ratio and others in the sections below.

3. POPULATING THE BLACK HOLE MASS GAPS: TIME EVOLVING CLUSTER MODEL

In this section we develop a simple time dependent cluster model to study the evolution of both 1G and 2G objects as a function of time. As further described in the following sections, in this model we take into account both binary and single dynamical ejections, and in particular the growth of 2G objects as a result of in-cluster 1G-1G mergers. We (still) assume the cluster is described by a fixed set v_d, n , and all objects have the same mass m , which of course is a simplification of a real cluster. This in turn however enables us to put forward simple, general, and informative statements, based solely on characteristic mass, length, and time scales.

In the first section below we derive a set of evolution equations for N_1 and N_2 , where N_i here denotes the number of objects of type ‘ i ’. In Sec. 3.2 we solve these equations from which we put upper limits on the ratio N_2/N_1 , illustrated for $m = 1.4M_\odot$ (2G in the LMG) and $m = 30M_\odot$ (2G in the UMG), for a grid of cluster systems described by v_d, n .

3.1. Evolution Equations

We consider a cluster described by a constant v_d, n that initially has a population of $N_1(0)$ 1G objects all with equal mass m . In this cluster there is a (time-dependent) population of binaries that interact with the

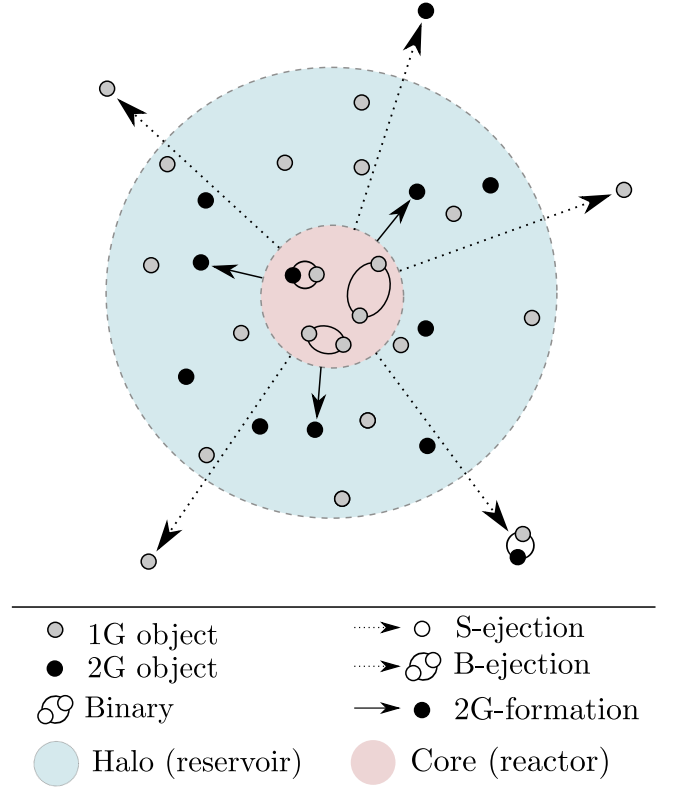


Figure 4. Illustration of the cluster model we use to study the formation of 2G-objects (*black dots*) through successive in-cluster GW mergers of 1G-objects (*grey dots*). The cluster is composed of two parts, an inner core (*pink region*) and an outer halo (*blue region*). Inside the core there is N_b binaries that interact with the flow of objects coming in from the outer halo. The resulting binary-single interactions are modeled using our δ -model described in Sec. 2.1, which leads to both dynamical ejections of binaries (*B-ejection*) and singles (*S-ejection*), and the production of 2G-objects (*2G-formation*) through in-cluster GW mergers of 1G-1G binaries. The number of 2G-objects compared to the number of 1G-objects, i.e. N_2/N_1 , after a Hubble time provides a rough estimate for how likely it is to observe a GW source from a binary merger that includes at least one 2G-object. We study the evolution of N_2/N_1 in Sec. 3, and comment on the implied possibility for populating the UMG and the LMG in Sec. 3.2.2.

surrounding single population, which give rise to dynamical ejections, exchanges, and in-cluster mergers. The absolute and relative number of N_1 (1G) and N_2 (2G) objects therefore changes over time through various dynamical mechanisms, that all depend on v_d, n, m . This configuration is described and illustrated in Fig. 4. The question is, for what initial conditions of v_d, n, m is the system able to produce a sizable population of 2G objects after a Hubble time? To answer this question, we start by writing out the following set of differential equations that we take to represent the evolution of N_1 and

N_2 ,

$$\begin{aligned}\dot{N}_1 &= - \left(\dot{N}_1^{ej} + \dot{N}_{21}^{ej} + 2\dot{N}_{11}^{ej} \right) - \left(\dot{N}_{21}^M + 2\dot{N}_{11}^M \right) \\ \dot{N}_2 &= - \left(\dot{N}_2^{ej} + \dot{N}_{21}^{ej} + 2\dot{N}_{22}^{ej} \right) - \left(\dot{N}_{21}^M + 2\dot{N}_{22}^M \right) \\ &\quad + \left(R_{11}^M \dot{N}_{11}^M \right),\end{aligned}\quad (24)$$

where N_i^{ej} is the number of objects of type ‘ i ’ (1G or 2G) that are ejected as singles, N_{ij}^{ej} is the number of ejected binaries consisting of object types ‘ $\{ij\}$ ’, N_{ij}^M is the number of ‘ $\{ij\}$ ’-binaries merging in-side the cluster, and R_{11}^M is the retention fraction of 1G-1G mergers. As seen, both ‘ejections’ (single and binary) and ‘in-cluster mergers’ all act as ‘sink terms’, except as for the term $\propto N_{11}^M$ that serves as the 2G ‘source term’. As we are studying the process of growing a 2G population through in-cluster GW mergers during successive ICs, we restrict our self in the following to describe systems that are able to undergo $N_c \gg 1$. Therefore, instead of evolving the above equations over e.g. individual interaction steps ‘ k ’, or time, we evolve them over the number of ICs, N_c . The ‘dot’ over each N refers therefore to the change per IC.

The relevant terms for writing out our evolution equations from above can be written as,

$$\dot{N}_i^{ej} \approx [N_b \bar{P}_M] p_i^{ej} N_s^{ej}, \quad (25)$$

$$\dot{N}_{ij}^{ej} \approx [N_b \bar{P}_M] p_{ij}^{ej}, \quad (26)$$

$$\dot{N}_{ij}^M \approx [N_b P_M] p_{ij}^b, \quad (27)$$

where N_b is the number of binaries, P_M ($\bar{P}_M = 1 - P_M$) is the integrated probability that a given binary does (not) merge during a single IC, p_i^{ej} is the probability that object ‘ i ’ is ejected after a binary-single interaction, N_s^{ej} is the total number of singles per binary ejected during one IC, p_{ij}^{ej} is the probability that binary-‘ $\{ij\}$ ’ is ejected after a binary-single interaction, and p_{ij}^b is the probability that ‘ $\{ij\}$ ’ is in a binary at a random hardening step ‘ k ’. These terms can be further expanded as,

$$p_2^{ej} \approx p_2^i p_{112}^{es} [1 + B], \quad p_1^{ej} \approx 1 - p_2^{ej} \quad (28)$$

$$p_{21}^{ej} \approx p_2^i p_{211}^{es} [1 + B], \quad p_{11}^{ej} \approx 1 - p_{21}^{ej} \quad (29)$$

$$p_{21}^b \approx p_2^i B, \quad p_{11}^b \approx 1 - p_{21}^b \quad (30)$$

$$p_{211}^{es} \approx 2w/3, \quad p_{112}^{es} \approx 1 - p_{211}^{es} \quad (31)$$

$$p_2^i \approx N_2 F / (N_1 + N_2), \quad p_1^i \approx 1 - p_2^i. \quad (32)$$

where p_2^i is the probability that object type ‘2’ (2G) is the incoming single object in a binary-single interaction at hardening step ‘ k ’, p_{ijk}^{es} is the probability that a given binary-single interaction results in an

endstate where ‘ $\{ij\}$ ’ is a binary and ‘ k ’ leaves as single, and $B = 2Fw/(3 - 2w)$. The factor F is introduced to quantify the probability ‘enhancement’ of a 2G-object to interact with a binary compared to a 1G-object. For example, the enhancement factor from standard gravitational focusing of having a 2G-object to interact with a binary compared to a 1G-object is $F = (1 + 1 + 2)/(1 + 1 + 1) = 4/3$. Similarly, w describes the ‘enhanced probability’ that the outcome of a binary-single interaction involving a 2G-object is ‘121’, i.e. where ‘12’ is a binary and ‘1’ is ejected as single. For this set of equations we have made four central assumptions: (1) All binary-single interactions involving objects ‘ $\{ijk\}$ ’ have the same outcome distributions irrespective of the initial configuration. (2) The probability to have interactions with > 1 2G-object is $= 0$, which follows from our considered limit of $N_2 \ll N_1$. (3) Dynamical single and binary ejections associated with a given interacting binary are only > 0 if the binary in question does not merge before concluding its IC. (4) All interactions and ICs follow our ‘ δ -model’ illustrated in Fig. 1. Now using these equations we can rewrite our evolution equations given by Eq. (24) as follows,

$$\begin{aligned}\dot{N}_1 &= N_b \times \left[+p_2^i (A - P_M(A - B)) - (N_t^{ej} - P_M N_s^{ej}) \right] \\ \dot{N}_2 &= N_b \times \left[-p_2^i (A - P_M(A - B)) + (p_{11}^b P_M R_{11}^M) \right],\end{aligned}\quad (33)$$

where $N_t^{ej} = 2 + N_s^{ej}$ is here the total number of ejected objects over 1 IC, and $A = [1 + B] (p_{112}^{es} N_s^{ej} + p_{211}^{es})$.

To summarize, our presented evolution equations given Eq. (24) are completely general, and shows simply what characteristic sink and source terms that are relevant for our problem. Other terms, such as strong binary-binary interactions (Zevin et al. 2019), and weak few-body scatterings (Hamers & Samsing 2019a; Samsing et al. 2019b; Hamers & Samsing 2019b, 2020), or more general mass-ratio dependent terms and corresponding GW kick prescriptions can be included, but this is beyond this paper. The resulting terms shown in Eq. (33) follow directly from simple combinatorics, and are constructed by calculating the (time dependent) probability for 1G- and 2G-objects to interact and exchange into the interactions states shown in Fig. 1, folded with the probability for dynamical ejections and in-cluster mergers during each IC. In the following sections we consider solutions to this coupled set of equations, from which we especially find a closed form solution to the upper limit on N_2/N_1 as a function of time.

3.2. Results

In the first section below, we study the evolution of N_1 and N_2 for two different cluster models, denoted cA

and cB , using the general set of evolution equations presented in the above Sec. 3.1. In the second section, we use these results to study the upper limit on the ratio N_2/N_1 evaluated at present day, i.e. at $t = t_H$, for a grid of v_d, n cluster systems.

3.2.1. Time-Evolving Populations

We study the evolution of N_1 and N_2 using Eq. (33) for two distinct cases, cA and cB . These two cases are described in the following.

Case ‘cA’: In this case we assume the weight factors $F = 1$ and $w = 1$, i.e., we keep track of the growing population of 2G-objects, but assume that in all dynamical aspects a 2G object is indistinguishable from a 1G object. We are therefore able to explore the effect from pure ‘combinatorics’ arising from the growing population of 2G-objects that are free to exchange, merge, and being ejected in the same way as the 1G objects. Using Eq. (33) with $F = 1, w = 1$ the evolution equations are in this case given by,

$$\begin{aligned}\dot{N}_1/N_b &\approx -p_1^i \left(N_t^{ej} - P_M N_s^{ej} \right) \\ \dot{N}_2/N_b &\approx -p_2^i \left(N_t^{ej} - P_M N_s^{ej} \right) + P_M R_{11}^M (1 - 2p_2^i),\end{aligned}\quad (34)$$

where we have used that under these assumptions $A = N_t^{ej}$ and $A - B = N_s^{ej}$. In this case the number of 2G-objects compared to 1G-objects present in the cluster after a Hubble time represents approximately a lower limit, as in ‘reality’ a higher number of 2G-objects will be left in the cluster due to their higher mass (e.g. Sigurdsson & Phinney 1993).

Case ‘cB’: In this case we assume that $p_2^i = 0$ and $R_{11}^M = 1$, i.e. that the 2G-objects are not participating in any interactions, and that the 1G-objects as a result dynamically evolve through interactions, merger, and ejections completely independent of the 2G-objects. As a result, the number of 2G-objects we here find after time t_H represents the highest number possible, and the 1G-population will also decrease to its lowest possible value. This case therefore represents the upper limit on how many 2G-objects one can keep in a cluster after time t_H compared to the 1G-population. The evolution equations are in this case given by Eq. (33) with $p_2^i = 0$ and $R_{11}^M = 1$,

$$\begin{aligned}\dot{N}_1/N_b &\approx - \left(N_t^{ej} - P_M N_s^{ej} \right) \\ \dot{N}_2/N_b &\approx + (P_M).\end{aligned}\quad (35)$$

This set of equations have a particular simple and interesting set of analytical solutions that we now explore before moving on. For this, we start by rewriting the

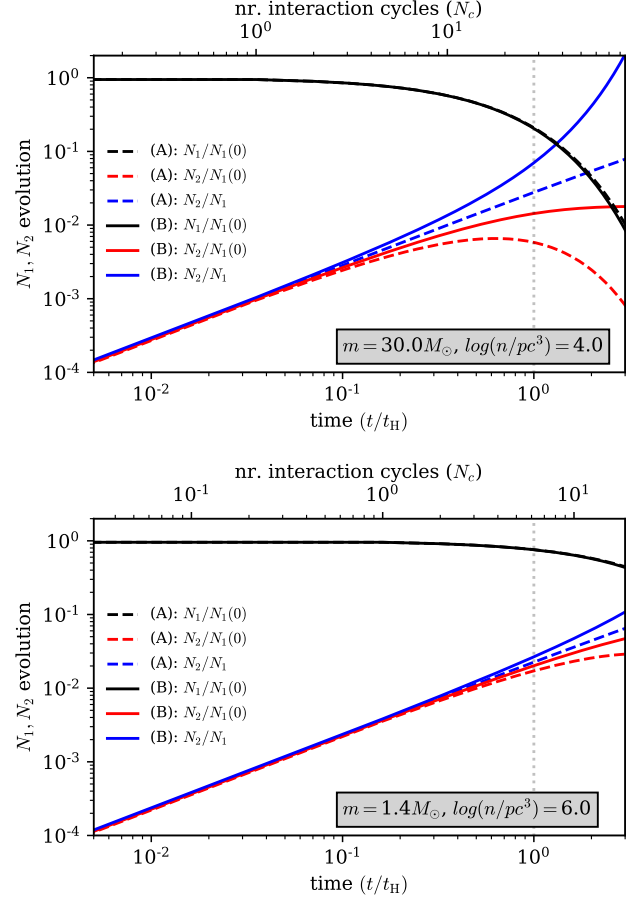


Figure 5. Re-scaled evolution of 1G-objects (black lines), $N_1/N_1(0)$, 2G-objects (red lines), $N_2/N_1(0)$, and their number ratio (blue lines), N_2/N_1 , as a function of time (lower x-axis), t/t_H , and corresponding number of ICs (upper x-axis), $N_c = t/\tau_m$. The dashed lines and solid lines show the solution from our cases cA and cB described in Sec. 3.2, respectively. For both plots we have assumed that $f_b = 0.01$, $N_t^{ej} = 6$, $v_d = 10 \text{ km s}^{-1}$, and $R_{11}^M = 1$, where the upper plot shows results for $m = 30 M_\odot$, and the lower plot for $m = 1.4 M_\odot$. In the $m = 30 M_\odot$ case the ratio N_2/N_1 approaches the 10%-level at $t/t_H \sim 1$ for our chosen parameters, which indicates that populating the UMG through in-cluster 1G-1G GW mergers seems possible. This is in contrast to the $1.4 M_\odot$ case, where n needs to take the relative high value of $n \sim 10^6 \text{ pc}^{-3}$ to even reach the 1%-level. This is further discussed in Sec. 3.2 and Sec. 3.2.2.

above equations into a more general form to shorten the notations: $\dot{N}_1 = -\alpha N_b$, $\dot{N}_2 = \beta N_b$, where we have defined,

$$\begin{aligned}\alpha &= N_t^{ej} - P_M N_s^{ej} \\ \beta &= P_M.\end{aligned}\quad (36)$$

To proceed, we now consider a specific model where the binary fraction stays constant such that $N_b = f_b \times N_1$. In this case, the solution to the above set of equations

is easily found from simple integrations, from which it follows,

$$\begin{aligned} N_1 &= N_1(0) \times \exp(-\alpha f_b N_c) \\ N_2 &= N_1(0) \times (\beta/\alpha) [1 - \exp(-\alpha f_b N_c)], \end{aligned} \quad (37)$$

where $N_1(0)$ is the initial number of 1G-objects, and $N_c = t/\tau_m$ is the number of ICs after time t . If we first consider the solution to N_1 , we see that the population of 1G-objects ‘decays’ over time as if the cluster represents a giant ‘radioactive nuclei’ with decay time t_{cd} , given by

$$t_{cd} \approx \frac{\tau_m}{\alpha f_b}, \quad (38)$$

where the time for undergoing one IC, τ_m , is given by Eq. (7). For example, for $a_m = a_{ej}$ the decay time is $t_{cd} \propto v_d^3/(nm^2 f_b)$, where we have used Eq. (4). One consequence of this model is that the decay rate, and thereby the number of 1G-objects N_1 after a Hubble time, depends exponentially on the binary fraction f_b . The binary fraction is at the moment unknown observationally, but numerical simulations of GCs using Monte-Carlo techniques have shown that it very likely stays constant with only small scatter around 1 – 5% (see e.g. Fig. 2 in Samsing et al. 2019a). As a result, a significant fraction of present day GCs likely have many of their 1G-objects left in their core, where the remaining fraction have lost its BHs through binary-single ‘evaporation’. This ‘evaporation effect’ will lead to a characteristic change in BBH merger rates as a function of redshift, similar to what is found for the set of GCs that ‘evaporates’ through tidal heating or direct tidal disruptions (e.g. Fragione & Kocsis 2018). Considering now N_2 for our model, we see that at early times $N_2 \approx N_1(0) f_b P_M N_c$, where we have used that $\exp(-ax) \approx 1 - ax$. This is expected, as this simply equals the number of mergers per IC evaluated for the initial $N_1(0)$ population ($N_1(0) f_b P_M$) times the number of ICs (N_c). Note that this is similar to Eq. (19), where we studied how effective a population consisting of a single binary ($1 = N_1(0) f_b$) is at growing a 2G-population. As N_c increases towards infinity, the N_2 population reaches a maximum ‘freeze-out value’, $\max(N_2)$, given by

$$\max(N_2) = N_1(0)(\beta/\alpha), \quad N_c \rightarrow \infty, \quad (39)$$

which interestingly do not depend on the binary fraction, although how fast N_2 reaches $\max(N_2)$ does. As seen, within a factor of unity, $\max(N_2)$ is simply given by the total number of binary mergers one would get if one turned the initial $N_1(0)$ population into a total of $N_1(0)/2$ binaries. Finally, if we now consider the number of 2G-objects relative to 1G-objects, one finds using

Eq. (37) that

$$N_2/N_1 = (\beta/\alpha) [\exp(\alpha f_b N_c) - 1]. \quad (40)$$

We see here that this ratio always increases, i.e., in this case there is no ‘freeze-out’ value. This of course originates from that N_1 keeps decreasing, whereas N_2 keeps increasing until it asymptotically reaches its value $\max(N_2)$. Considering the limit where $N_2/N_1 = 1$, we can solve for the corresponding characteristic N_c scale, denoted here by N_c^{2E1} ,

$$N_c^{2E1} = \frac{\ln(1 + \alpha/\beta)}{\alpha f_b}, \quad (41)$$

which equals the number of IC cycles, or time $t_c^{2E1} \approx N_c^{2E1} \times \tau_m$, it takes for N_2 to be similar to N_1 . Comparing t_c^{2E1} with t_H provides a rough estimate for when a system is effective in growing a sizable 2G-population within a Hubble time. We will study the ratio N_2/N_1 from cB in greater detail in Sec. 3.2.2 below.

The evolution of N_1 and N_2 for case cA and cB as a function of time is shown in Fig. 5 assuming the binary fraction stays constant at $f_b = 0.01$, $N_t^{ej} = 6$, $N_s^{ej} = 4$, $v_d = 10 \text{ km s}^{-1}$, and $R_M^{11} = 1$. Note here that in the upper plot where $m = 30M_\odot$ the density is $n = 10^4 \text{ pc}^{-3}$, whereas in the lower plot for $m = 1.4M_\odot$ the density is instead $n = 10^6 \text{ pc}^{-3}$, as this is around the threshold for when $N_c \gg 1$ (see Fig. 2). Starting with cA , we see in the $m = 30M_\odot$ case how the 2G-population first grows steadily up to a given point just before $t = t_H$, after which it starts decreasing. This decrease is sourced by the binary and single ejection sink terms from Eq. (34). Considering now N_2/N_1 , we see that at $t = t_H$ this ratio is (only) at the 1%-level. We therefore expect N_2/N_1 to be of that order or greater for these cluster values, depending on the retention fraction R_M^{11} . The same characteristics are true for the $m = 1.4M_\odot$ case, but to reach a value for N_2/N_1 of a few percent, we see that n in this case has to be of order 10^6 pc^{-3} , which is much higher than what is found in most astrophysical systems. Considering now cB , it is seen for $m = 30M_\odot$ that N_1 decays exponentially, whereas N_2 steadily levels off at its ‘freeze-out value’ given by Eq. (39). The characteristic time given by Eq. (41) for which $N_2 = N_1$ is only $2 \sim 3$ times t_H , and as a result, the ratio N_2/N_1 approaches here the 10%-level at t_H . This indicates that $\gtrsim 30M_\odot$ COs are able to reach interesting limits when it comes to populating the UMG, whereas in the $\sim 1M_\odot$ CO case, it seems very difficult to undergo enough in-cluster mergers to populate the LMG. We will study this in greater detail in the section below.

3.2.2. Upper Limits on 2G-Objects

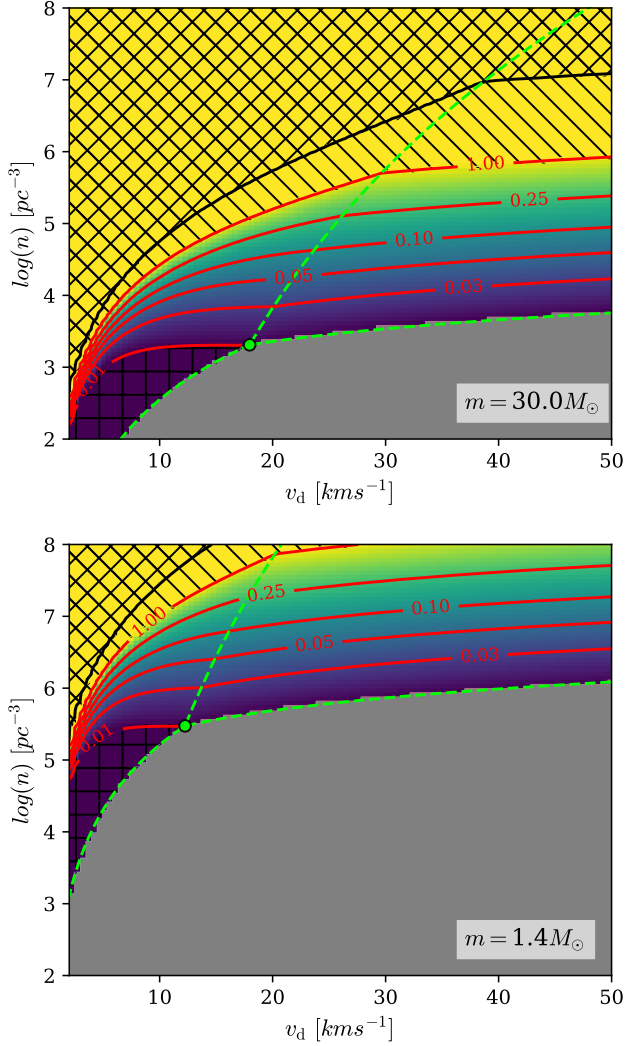


Figure 6. Results from our considered case *cB* described in Sec. 3.2.1, where the number of 1G- and 2G-object as a function of time is given by Eq. (37), and their ratio N_2/N_1 by Eq. (40). We here consider solutions to $t = t_H$ for a model described by $f_b = 0.01$, $R_M^1 = 1$, $N_t^{ej} = 6$, and $N_s^{ej} = 4$, where the *upper* and *lower* plots correspond to $m = 30M_\odot$ and $m = 1.4M_\odot$, respectively. The area covered by the *red contours* is where $0.01 < N_2/N_1 < 1.0$, i.e. it is the region that gives rise to both consistent (< 1.0) and interesting (> 0.01) outcomes for growing a 2G-population. In the *yellow ‘\’-hatched area*, our formalism evaluated at $t = t_H$ breaks down as N_2 is here $> N_1$, where in the *grey area* our N_c averaging approach breaks down as N_c is here < 1 . In the *yellow ‘X’-hatched area* $N_1/N_1(0) < 10^{-4}$; therefore, if a system is located within this area it will ‘evaporate’ within a Hubble time if its initial number of BHs is $\lesssim 10^4$. The ‘+’-hatched area is where $N_2/N_1 < 0.01$ and $N_c \gg 1$, and highlights therefore systems that clearly undergo several ICs, but still end up with a relative small 2G-population. The green separation lines are describe in Sec. 2.2.1. Results related to this figure are described in Sec. 3.2.2.

Fig. 6 shows results related to the ratio N_2/N_1 given by Eq. (40) evaluated at $t = t_H$, as further described in the figure caption. As described in Sec. 3.2.1, this case represents in our model an upper limit on N_2/N_1 . Considering first the upper plot showing the $m = 30M_\odot$ case, we see that for a GC with $v_d \sim 10 \text{ km s}^{-1}$ a population of 1G-objects can over a Hubble time turn into a population with $N_2/N_1 > 0.1$ if $n \gtrsim 10^4 \text{ pc}^{-3}$. Although this is an upper limit, it greatly illustrates that the length, mass, and times scales associated with a typical cluster hosting BHs of mass $\sim 30M_\odot$ in the core is able to populate the upper mass gap through successive mergers of its 1G-population. Considering now the lower plot showing results for the $1.4M_\odot$ case, we see that for $v_d \sim 10 \text{ km s}^{-1}$ the density has to be $\gtrsim 10^5 \text{ pc}^{-3}$ to even grow a 2G-population with $N_2/N_1 > 0.01$, and $\gtrsim 10^6 \text{ pc}^{-3}$ for $N_2/N_1 > 0.1$. From this we conclude that populating the lower mass gap through successive mergers of NSs in any reasonable astrophysical cluster seems almost impossible, not even when we assume that the entire population is consisting of only NSs. This last assumption is in fact also highly optimistic, as NSs will not segregate and form their own sub-cluster in the same way as BHs because their characteristic $1.4M_\odot$ mass is very close to that of the ordinary stars in the cluster. As a result, NSs will exchange and interact frequently with the stellar population, which introduces ‘impurities’ in the IC illustrated in Fig. 1. The probability that two NSs merge inside the cluster is therefore significantly smaller than what we have assumed in our considered *cB* scenario. In comparison, the BHs have such a large mass compared to the remaining stellar population, that they easily form their own sub-system (e.g. Askar et al. 2018). In Fig. 7 we show how these results depend more broadly on the mass m , where we show N_2/N_1 from case *cB*, as a function of m for $n = 10^4 \text{ pc}^{-3}$ (top plot) and $n = 10^5 \text{ pc}^{-3}$ (bottom plot), and two different binary fractions, as further described in the figure caption.

Finally, we note that the real ‘bottle neck’ in populating the lower mass gap is not directly related to the probability P_M per IC for a NS population to undergo NS-NS mergers inside their cluster. Instead, it is the time it takes for a NS-NS binary to undergo one IC, τ_m , that simply is too long for a standard cluster. This is clear from Fig. 6, as the grey area, where $N_c \lesssim 1$, sets the lower limit at $n = 10^5 \text{ pc}^{-3}$ for 10 km s^{-1} . In the limit where $a_m = a_{ej}$ the number of ICs evaluated at

t_H , $N_c(t_H) = t_H/\tau_m(a_{ej})$, is given by,

$$N_c(t_H) \approx t_H \left[\frac{\pi G^2 \Delta^2}{\delta f_{ed}^2} \right] \times \frac{nm^2}{v_d^3} \quad (42)$$

$$\approx 0.8 \left(\frac{n}{10^5 pc^{-3}} \right) \left(\frac{m}{1.4 M_\odot} \right)^2 \left(\frac{v_d}{10 km s^{-1}} \right)^{-3}, \quad (43)$$

and is indeed just around unity for NS-NS binaries for our chosen normalizations. It is furthermore seen that $N_c(t_H)$ rapidly decreases with mass m as $\propto m^2$. However, as seen on Fig. 3, if the system is in the area for which $N_c(t_H) > 1$, the dependence on m on how many in-cluster mergers a given binary can produce within a Hubble time, $N'_M(t_H)$, is less sensitive to m , as $N_c(t_H) \times P_m \propto m^{8/7}$. All in all, the limit for which $N_c(t_H) = 1$ plays therefore a crucial role for determining what systems that are able to produce a significant 2G-population. We conclude our study below.

4. CONCLUSIONS

We have in this paper studied the formation of 2G objects formed through 1G-1G in-cluster mergers in dense clusters. We have in particular explored the possibility for populating the LMG ($3 - 5 M_\odot$) and the UMG ($\gtrsim 45 M_\odot$) through the merger of BNSs and BBHs, respectively. Understanding what cluster systems that are able to populate these two mass-gaps has wide implications for both GW astrophysics and stellar physics. For example, if nature is proven not to be able to create mass-gap BHs through normal stellar evolution, then current and future measures of the BH mass spectrum, through e.g. GW observations, will give us insight into the formation mechanisms of BBH mergers in clusters. On the other hand, if observations hint that stellar clusters do not contribute significantly to the observed GW merger rate, e.g. through independent measures of the fraction of eccentric BBH mergers (e.g. Samsing 2018), then an observed population of mass-gap objects will hint that our single stellar models need to be revised. For these reasons, several new studies have discussed the possibility for dynamically populating these mass gaps (e.g. O'Leary et al. 2016; Fishbach et al. 2017; Gerosa & Berti 2017; Yang et al. 2019; Antonini et al. 2019; Gerosa & Berti 2019; Samsing & Ilan 2019; Rodriguez et al. 2019; Gerosa et al. 2020; Safarzadeh et al. 2020; Gayathri et al. 2020; Kimball et al. 2020; Doctor et al. 2020; Baibhav et al. 2020).

Through a fully analytical approach we have here studied how efficient a cluster, described by a constant v_d, n , can turn its initial population of N_1 1G-objects into a sizable population of N_2 2G-objects through in-cluster GW mergers. We have in particular explored the

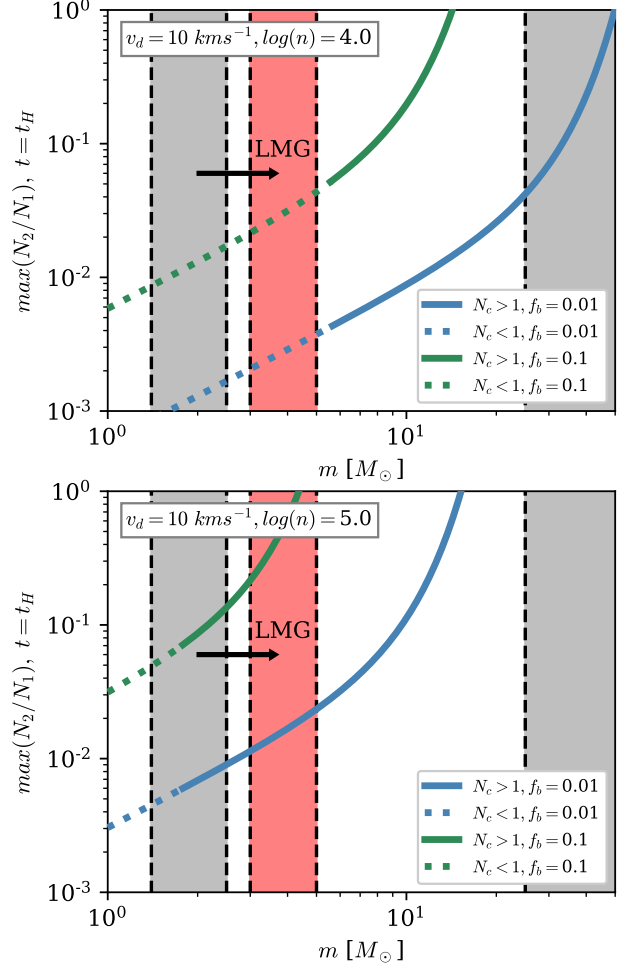


Figure 7. Number of 2G-objects (N_2) relative to 1G-objects (N_1) derived for our case cB using Eq. (40) at $t = t_H$, as a function of m for fixed v_d , but varying n and f_b , as further indicated in the legends. The two plots differ by the value of n , where $n = 10^4 pc^{-3}$ and $n = 10^5 pc^{-3}$ in the upper and lower plots, respectively. The grey bands show the mass range for which a merger that produces a remnant with mass $\sim 2m$ will land in the corresponding mass gap, where the red band shows the LMG (the UMG is not shown). For example, a merger between two COs (NSs) in the lower grey band will form a merger product that lands in the red LMG band, as further illustrated by the black arrow. The dotted lines highlight the part of the curves for which $N_c < 1$ (2G formation is highly ineffective), where the solid lines correspond to $N_c > 1$ (2G formation is possible).

upper limit on the ratio N_2/N_1 evaluated after a Hubble time, as a function of v_d, n and m (Sec. 3.2.2). Our limit is based entirely on dynamics, and complements therefore greatly the recent study by Gerosa & Berti (2019), where the limit was derived from considering the magnitude of GW kicks. From our analysis we have reached the following conclusions:

Populating the LMG through in-cluster mergers of BNSs is a very slow process for any astrophysical cluster. For example, as shown in Fig. 6, even in the highly idealized case of a GC core populated entirely by NSs, the number density n has to be $> 10^6 \text{ pc}^{-3}$ to reach $N_2/N_1 \sim 0.1$. As discussed in Sec. 3.2.2, not only is this density much higher than what is found for real clusters, but NSs are also likely to mix with other stars due to their similar mass, which reduces their in-cluster merger probability further. In fact, our results show that what really limits a NS rich core to undergo enough in-cluster mergers to populate the LMG is actually the timescale for interactions, and not how the NSs exactly merge inside their cluster. This is seen in Fig. 6, where for a NS dominated core (bottom plot) a density of $n \gtrsim 10^5 \text{ pc}^{-3}$ for $v_d \sim 10 \text{ kms}^{-1}$ is required to move above the grey area, i.e. for a BNS to undergo at least 1 IC. In our described ‘standard picture’ of dynamically assembled in-cluster mergers (Sec. 2.1), an efficient production of LMG objects is therefore highly unlikely. If clusters for some reason are still observed to effectively produce LMG objects through dynamics, then more ‘exotic’ dynamical pathways have to be evoked. Alternatively, it could be that some clusters start out with a high BNS fraction (see Fig. 7) that would lead to a relative high number of 2G objects after a Hubble time. However, in that case, there would still be problems related to how fast this 2G population can be dynamically paired up with other COs to undergo, say, observable GW mergers. Therefore, observing GW sources with at least one LMG object formed in a cluster near the grey area in Fig. 6 (bottom) seems therefore highly unlikely.

Populating the UMG is in comparison much easier, e.g., in Fig. 6 (top) it is clearly seen that reaching values of $N_2/N_1 \sim 0.1$ only requires clusters with a central density of $\sim 10^4 \text{ pc}^{-3}$. This is a much more reasonable magnitude, which leads us to conclude that populating the UMG in clusters is relatively easy, at least dynamically, without introducing any non-standard pathways. Our model even implies that for $n \gtrsim 10^4 \text{ pc}^{-3}$ there is high probability for the initial 1G population to turn almost entirely into a 2G population. Our models are not able to accurately describe this scenario, but it does

at least hint that in moderate dense clusters in-cluster mergers can be highly effective in changing the initial mass function. This has great implications for 3. generation GW observations where will see every BBH merger within our observable patch as a function of redshift.

Finally, we note that a few studies that were completed while our present study was underway point towards similar conclusions to what we have here. For example, in Ye et al. (2020) it was shown using a fully numerical approach that the rate of BNS mergers originating from GCs is low, where both Rodriguez et al. (2019) and Baibhav et al. (2020) illustrated that populating the UMG definitely seems possible. However, other studies still keep the question open to what degree the LMG can be populated in clusters (e.g. Gupta et al. 2020). The topic is therefore highly rich and interesting, and our study greatly compliments this recent literature with the first set of closed form solutions that encapsulate all the correct scalings and relations of the problem. We note here that standard brute-force N -body techniques are still too slow at evolving high density clusters, which is why we and others explore how to solve this problem using approximate schemes (see also work by Antonini et al. (2019); Antonini & Gieles (2020)). We are currently working on a self consistent hybrid scheme that will enable us to correctly evolve a full mass distribution. Our present paper plays a crucial role in providing the first steps in this highly relevant and timely topic.

ACKNOWLEDGMENTS

The authors thank the Yukawa Institute for Theoretical Physics at Kyoto University, and the organizers of the workshop YKIS2019 ‘Black Holes and Neutron Stars with Gravitational Waves’, where many useful conversations took place. It is also a pleasure to thank Kyle Kremer for enlightening discussions. JS acknowledges support from the Lyman Spitzer Fellowship and the European Unions Horizon 2020 research and innovation programme under the Marie Skłodowska-Curie grant agreement No. 844629. KH acknowledges support from the Lyman Spitzer Fellowship.

REFERENCES

- Aarseth, S. J., & Heggie, D. C. 1976, *A&A*, 53, 259
- Abbott, B. P., Abbott, R., Abbott, T. D., et al. 2016a, *Physical Review Letters*, 116, 061102, doi: [10.1103/PhysRevLett.116.061102](https://doi.org/10.1103/PhysRevLett.116.061102)
- . 2016b, *Physical Review Letters*, 116, 241103, doi: [10.1103/PhysRevLett.116.241103](https://doi.org/10.1103/PhysRevLett.116.241103)
- . 2016c, *Physical Review X*, 6, 041015, doi: [10.1103/PhysRevX.6.041015](https://doi.org/10.1103/PhysRevX.6.041015)

- . 2017a, *Physical Review Letters*, 118, 221101, doi: [10.1103/PhysRevLett.118.221101](https://doi.org/10.1103/PhysRevLett.118.221101)
- . 2017b, *Physical Review Letters*, 119, 141101, doi: [10.1103/PhysRevLett.119.141101](https://doi.org/10.1103/PhysRevLett.119.141101)
- . 2017c, *Physical Review Letters*, 119, 161101, doi: [10.1103/PhysRevLett.119.161101](https://doi.org/10.1103/PhysRevLett.119.161101)
- Andrews, J. J., & Mandel, I. 2019, *ApJL*, 880, L8, doi: [10.3847/2041-8213/ab2ed1](https://doi.org/10.3847/2041-8213/ab2ed1)
- Antonini, F., Chatterjee, S., Rodriguez, C. L., et al. 2016, *ApJ*, 816, 65, doi: [10.3847/0004-637X/816/2/65](https://doi.org/10.3847/0004-637X/816/2/65)
- Antonini, F., & Gieles, M. 2020, *MNRAS*, 492, 2936, doi: [10.1093/mnras/stz3584](https://doi.org/10.1093/mnras/stz3584)
- Antonini, F., Gieles, M., & Gualandris, A. 2019, *MNRAS*, 486, 5008, doi: [10.1093/mnras/stz1149](https://doi.org/10.1093/mnras/stz1149)
- Antonini, F., & Rasio, F. A. 2016, *ApJ*, 831, 187, doi: [10.3847/0004-637X/831/2/187](https://doi.org/10.3847/0004-637X/831/2/187)
- Antonini, F., Rodriguez, C. L., Petrovich, C., & Fischer, C. L. 2018, *MNRAS*, 480, L58, doi: [10.1093/mnrasl/sly126](https://doi.org/10.1093/mnrasl/sly126)
- Antonini, F., Toonen, S., & Hamers, A. S. 2017, *ApJ*, 841, 77, doi: [10.3847/1538-4357/aa6f5e](https://doi.org/10.3847/1538-4357/aa6f5e)
- Askar, A., Arca Sedda, M., & Giersz, M. 2018, *MNRAS*, 478, 1844, doi: [10.1093/mnras/sty1186](https://doi.org/10.1093/mnras/sty1186)
- Askar, A., Szkudlarek, M., Gondek-Rosińska, D., Giersz, M., & Bulik, T. 2017, *MNRAS*, 464, L36, doi: [10.1093/mnrasl/slw177](https://doi.org/10.1093/mnrasl/slw177)
- Bae, Y.-B., Kim, C., & Lee, H. M. 2014, *MNRAS*, 440, 2714, doi: [10.1093/mnras/stu381](https://doi.org/10.1093/mnras/stu381)
- Baibhav, V., Gerosa, D., Berti, E., et al. 2020, *arXiv e-prints*, arXiv:2004.00650. <https://arxiv.org/abs/2004.00650>
- Bailyn, C. D., Jain, R. K., Coppi, P., & Orosz, J. A. 1998, *ApJ*, 499, 367, doi: [10.1086/305614](https://doi.org/10.1086/305614)
- Banerjee, S., Baumgardt, H., & Kroupa, P. 2010, *MNRAS*, 402, 371, doi: [10.1111/j.1365-2966.2009.15880.x](https://doi.org/10.1111/j.1365-2966.2009.15880.x)
- Bartos, I., Kocsis, B., Haiman, Z., & Márka, S. 2017, *ApJ*, 835, 165, doi: [10.3847/1538-4357/835/2/165](https://doi.org/10.3847/1538-4357/835/2/165)
- Belczynski, K., Holz, D. E., Bulik, T., & O’Shaughnessy, R. 2016a, *Nature*, 534, 512, doi: [10.1038/nature18322](https://doi.org/10.1038/nature18322)
- Belczynski, K., Repetto, S., Holz, D. E., et al. 2016b, *ApJ*, 819, 108, doi: [10.3847/0004-637X/819/2/108](https://doi.org/10.3847/0004-637X/819/2/108)
- Berti, E., Cardoso, V., Gonzalez, J. A., et al. 2007, *PhRvD*, 76, 064034, doi: [10.1103/PhysRevD.76.064034](https://doi.org/10.1103/PhysRevD.76.064034)
- Bird, S., Cholis, I., Muñoz, J. B., et al. 2016, *Physical Review Letters*, 116, 201301, doi: [10.1103/PhysRevLett.116.201301](https://doi.org/10.1103/PhysRevLett.116.201301)
- Carr, B., Kühnel, F., & Sandstad, M. 2016, *PhRvD*, 94, 083504, doi: [10.1103/PhysRevD.94.083504](https://doi.org/10.1103/PhysRevD.94.083504)
- Chen, X., & Amaro-Seoane, P. 2017, *ApJL*, 842, L2, doi: [10.3847/2041-8213/aa74ce](https://doi.org/10.3847/2041-8213/aa74ce)
- Cholis, I., Kovetz, E. D., Ali-Haïmoud, Y., et al. 2016, *PhRvD*, 94, 084013, doi: [10.1103/PhysRevD.94.084013](https://doi.org/10.1103/PhysRevD.94.084013)
- Doctor, Z., Wysocki, D., O’Shaughnessy, R., Holz, D. E., & Farr, B. 2020, *ApJ*, 893, 35, doi: [10.3847/1538-4357/ab7fac](https://doi.org/10.3847/1538-4357/ab7fac)
- Dominik, M., Belczynski, K., Fryer, C., et al. 2012, *ApJ*, 759, 52, doi: [10.1088/0004-637X/759/1/52](https://doi.org/10.1088/0004-637X/759/1/52)
- . 2013, *ApJ*, 779, 72, doi: [10.1088/0004-637X/779/1/72](https://doi.org/10.1088/0004-637X/779/1/72)
- Dominik, M., Berti, E., O’Shaughnessy, R., et al. 2015, *ApJ*, 806, 263, doi: [10.1088/0004-637X/806/2/263](https://doi.org/10.1088/0004-637X/806/2/263)
- D’Orazio, D. J., & Loeb, A. 2017, *ArXiv e-prints*. <https://arxiv.org/abs/1706.04211>
- Farmer, R., Renzo, M., de Mink, S. E., Marchant, P., & Justham, S. 2019, *ApJ*, 887, 53, doi: [10.3847/1538-4357/ab518b](https://doi.org/10.3847/1538-4357/ab518b)
- Farr, W. M., Fishbach, M., Ye, J., & Holz, D. E. 2019, *ApJL*, 883, L42, doi: [10.3847/2041-8213/ab4284](https://doi.org/10.3847/2041-8213/ab4284)
- Farr, W. M., Sravan, N., Cantrell, A., et al. 2011, *ApJ*, 741, 103, doi: [10.1088/0004-637X/741/2/103](https://doi.org/10.1088/0004-637X/741/2/103)
- Fishbach, M., Holz, D. E., & Farr, B. 2017, *ApJL*, 840, L24, doi: [10.3847/2041-8213/aa7045](https://doi.org/10.3847/2041-8213/aa7045)
- Fragione, G., & Bromberg, O. 2019, *arXiv e-prints*, arXiv:1903.09659. <https://arxiv.org/abs/1903.09659>
- Fragione, G., & Kocsis, B. 2018, *PhRvL*, 121, 161103, doi: [10.1103/PhysRevLett.121.161103](https://doi.org/10.1103/PhysRevLett.121.161103)
- . 2019, *MNRAS*, 486, 4781, doi: [10.1093/mnras/stz1175](https://doi.org/10.1093/mnras/stz1175)
- . 2020, *MNRAS*, 493, 3920, doi: [10.1093/mnras/staa443](https://doi.org/10.1093/mnras/staa443)
- Fragione, G., & Loeb, A. 2019, *MNRAS*, 486, 4443, doi: [10.1093/mnras/stz1131](https://doi.org/10.1093/mnras/stz1131)
- Gayathri, V., Bartos, I., Haiman, Z., et al. 2020, *ApJL*, 890, L20, doi: [10.3847/2041-8213/ab745d](https://doi.org/10.3847/2041-8213/ab745d)
- Gerosa, D., & Berti, E. 2017, *PhRvD*, 95, 124046, doi: [10.1103/PhysRevD.95.124046](https://doi.org/10.1103/PhysRevD.95.124046)
- . 2019, *PhRvD*, 100, 041301, doi: [10.1103/PhysRevD.100.041301](https://doi.org/10.1103/PhysRevD.100.041301)
- Gerosa, D., Vitale, S., & Berti, E. 2020, *arXiv e-prints*, arXiv:2005.04243. <https://arxiv.org/abs/2005.04243>
- Giersz, M., Leigh, N., Hypki, A., Lützgendorf, N., & Askar, A. 2015, *MNRAS*, 454, 3150, doi: [10.1093/mnras/stv2162](https://doi.org/10.1093/mnras/stv2162)
- Gültekin, K., Miller, M. C., & Hamilton, D. P. 2004, *ApJ*, 616, 221
- . 2006, *ApJ*, 640, 156
- Gupta, A., Gerosa, D., Arun, K. G., et al. 2020, *PhRvD*, 101, 103036, doi: [10.1103/PhysRevD.101.103036](https://doi.org/10.1103/PhysRevD.101.103036)
- Hamers, A. S., Bar-Or, B., Petrovich, C., & Antonini, F. 2018, *ApJ*, 865, 2, doi: [10.3847/1538-4357/aadae2](https://doi.org/10.3847/1538-4357/aadae2)
- Hamers, A. S., & Samsing, J. 2019a, *MNRAS*, 487, 5630, doi: [10.1093/mnras/stz1646](https://doi.org/10.1093/mnras/stz1646)
- . 2019b, *MNRAS*, 488, 5192, doi: [10.1093/mnras/stz2029](https://doi.org/10.1093/mnras/stz2029)
- . 2020, *MNRAS*, 494, 850, doi: [10.1093/mnras/staa691](https://doi.org/10.1093/mnras/staa691)

- Hamers, A. S., & Thompson, T. A. 2019, *ApJ*, 883, 23, doi: [10.3847/1538-4357/ab3b06](https://doi.org/10.3847/1538-4357/ab3b06)
- Heggie, D. C. 1975, *MNRAS*, 173, 729
- Hénault-Brunet, V., Gieles, M., Strader, J., et al. 2020, *MNRAS*, 491, 113, doi: [10.1093/mnras/stz2995](https://doi.org/10.1093/mnras/stz2995)
- Hoang, B.-M., Naoz, S., Kocsis, B., Rasio, F. A., & Dosopoulou, F. 2017, *ArXiv e-prints*. <https://arxiv.org/abs/1706.09896>
- Hong, J., & Lee, H. M. 2015, *MNRAS*, 448, 754, doi: [10.1093/mnras/stv035](https://doi.org/10.1093/mnras/stv035)
- Hotokezaka, K., & Piran, T. 2017, *ApJ*, 842, 111, doi: [10.3847/1538-4357/aa6f61](https://doi.org/10.3847/1538-4357/aa6f61)
- Hut, P., & Bahcall, J. N. 1983, *ApJ*, 268, 319
- Janiuk, A., Bejger, M., Charzyński, S., & Sukova, P. 2017, *ArXiv e-prints*, 51, 7, doi: [10.1016/j.newast.2016.08.002](https://doi.org/10.1016/j.newast.2016.08.002)
- Kalogera, V. 2000, *ApJ*, 541, 319, doi: [10.1086/309400](https://doi.org/10.1086/309400)
- Kimball, C., Talbot, C., Berry, C. P. L., et al. 2020, *arXiv e-prints*, arXiv:2005.00023. <https://arxiv.org/abs/2005.00023>
- Kinugawa, T., Inayoshi, K., Hotokezaka, K., Nakauchi, D., & Nakamura, T. 2014, *MNRAS*, 442, 2963, doi: [10.1093/mnras/stu1022](https://doi.org/10.1093/mnras/stu1022)
- Kızıltan, B., Baumgardt, H., & Loeb, A. 2017, *Nature*, 542, 203, doi: [10.1038/nature21361](https://doi.org/10.1038/nature21361)
- Kremer, K., Lu, W., Rodriguez, C. L., Lachat, M., & Rasio, F. A. 2019a, *ApJ*, 881, 75, doi: [10.3847/1538-4357/ab2e0c](https://doi.org/10.3847/1538-4357/ab2e0c)
- Kremer, K., Ye, C. S., Chatterjee, S., Rodriguez, C. L., & Rasio, F. A. 2020, in *IAU Symposium*, Vol. 351, IAU Symposium, ed. A. Bragaglia, M. Davies, A. Sills, & E. Vesperini, 357–366, doi: [10.1017/S1743921319007269](https://doi.org/10.1017/S1743921319007269)
- Kremer, K., Rodriguez, C. L., Amaro-Seoane, P., et al. 2019b, *PhRvD*, 99, 063003, doi: [10.1103/PhysRevD.99.063003](https://doi.org/10.1103/PhysRevD.99.063003)
- Leung, S.-C., Nomoto, K., & Blinnikov, S. 2019, *ApJ*, 887, 72, doi: [10.3847/1538-4357/ab4fe5](https://doi.org/10.3847/1538-4357/ab4fe5)
- Liu, B., & Lai, D. 2017, *ApJL*, 846, L11, doi: [10.3847/2041-8213/aa8727](https://doi.org/10.3847/2041-8213/aa8727)
- . 2018, *ApJ*, 863, 68, doi: [10.3847/1538-4357/aad09f](https://doi.org/10.3847/1538-4357/aad09f)
- . 2019, *MNRAS*, 483, 4060, doi: [10.1093/mnras/sty3432](https://doi.org/10.1093/mnras/sty3432)
- Liu, B., Lai, D., & Wang, Y.-H. 2019, *ApJ*, 881, 41, doi: [10.3847/1538-4357/ab2dfb](https://doi.org/10.3847/1538-4357/ab2dfb)
- Loeb, A. 2016, *ApJL*, 819, L21, doi: [10.3847/2041-8205/819/2/L21](https://doi.org/10.3847/2041-8205/819/2/L21)
- Lopez, Martin, J., Batta, A., Ramirez-Ruiz, E., Martinez, I., & Samsing, J. 2019, *ApJ*, 877, 56, doi: [10.3847/1538-4357/ab1842](https://doi.org/10.3847/1538-4357/ab1842)
- McKernan, B., Ford, K. E. S., Bellovary, J., et al. 2017, *ArXiv e-prints*. <https://arxiv.org/abs/1702.07818>
- Miller, M. C., & Davies, M. B. 2012, *ApJ*, 755, 81, doi: [10.1088/0004-637X/755/1/81](https://doi.org/10.1088/0004-637X/755/1/81)
- Murguia-Berthier, A., MacLeod, M., Ramirez-Ruiz, E., Antoni, A., & Macias, P. 2017, *ApJ*, 845, 173, doi: [10.3847/1538-4357/aa8140](https://doi.org/10.3847/1538-4357/aa8140)
- Naoz, S. 2016, *ARA&A*, 54, 441, doi: [10.1146/annurev-astro-081915-023315](https://doi.org/10.1146/annurev-astro-081915-023315)
- Naoz, S., Kocsis, B., Loeb, A., & Yunes, N. 2013, *ApJ*, 773, 187, doi: [10.1088/0004-637X/773/2/187](https://doi.org/10.1088/0004-637X/773/2/187)
- O’Leary, R. M., Kocsis, B., & Loeb, A. 2009, *MNRAS*, 395, 2127, doi: [10.1111/j.1365-2966.2009.14653.x](https://doi.org/10.1111/j.1365-2966.2009.14653.x)
- O’Leary, R. M., Meiron, Y., & Kocsis, B. 2016, *ApJL*, 824, L12, doi: [10.3847/2041-8205/824/1/L12](https://doi.org/10.3847/2041-8205/824/1/L12)
- Özel, F., Psaltis, D., Narayan, R., & McClintock, J. E. 2010, *ApJ*, 725, 1918, doi: [10.1088/0004-637X/725/2/1918](https://doi.org/10.1088/0004-637X/725/2/1918)
- Park, D., Kim, C., Lee, H. M., Bae, Y.-B., & Belczynski, K. 2017, *MNRAS*, 469, 4665, doi: [10.1093/mnras/stx1015](https://doi.org/10.1093/mnras/stx1015)
- Piran, Z., & Piran, T. 2020, *ApJ*, 892, 64, doi: [10.3847/1538-4357/ab792a](https://doi.org/10.3847/1538-4357/ab792a)
- Portegies Zwart, S. F., & McMillan, S. L. W. 2000, *ApJ*, 528, L17
- Randall, L., & Xianyu, Z.-Z. 2018a, *ApJ*, 864, 134, doi: [10.3847/1538-4357/aad7fe](https://doi.org/10.3847/1538-4357/aad7fe)
- . 2018b, *ApJ*, 853, 93, doi: [10.3847/1538-4357/aaa1a2](https://doi.org/10.3847/1538-4357/aaa1a2)
- Rodriguez, C. L., Amaro-Seoane, P., Chatterjee, S., et al. 2018, *PhRvD*, 98, 123005, doi: [10.1103/PhysRevD.98.123005](https://doi.org/10.1103/PhysRevD.98.123005)
- Rodriguez, C. L., & Antonini, F. 2018, *ApJ*, 863, 7, doi: [10.3847/1538-4357/aacea4](https://doi.org/10.3847/1538-4357/aacea4)
- Rodriguez, C. L., Chatterjee, S., & Rasio, F. A. 2016a, *PhRvD*, 93, 084029, doi: [10.1103/PhysRevD.93.084029](https://doi.org/10.1103/PhysRevD.93.084029)
- Rodriguez, C. L., Haster, C.-J., Chatterjee, S., Kalogera, V., & Rasio, F. A. 2016b, *ApJL*, 824, L8, doi: [10.3847/2041-8205/824/1/L8](https://doi.org/10.3847/2041-8205/824/1/L8)
- Rodriguez, C. L., Morscher, M., Pattabiraman, B., et al. 2015, *Physical Review Letters*, 115, 051101, doi: [10.1103/PhysRevLett.115.051101](https://doi.org/10.1103/PhysRevLett.115.051101)
- Rodriguez, C. L., Zevin, M., Amaro-Seoane, P., et al. 2019, *PhRvD*, 100, 043027, doi: [10.1103/PhysRevD.100.043027](https://doi.org/10.1103/PhysRevD.100.043027)
- Rodriguez, C. L., Zevin, M., Pankow, C., Kalogera, V., & Rasio, F. A. 2016c, *ApJL*, 832, L2, doi: [10.3847/2041-8205/832/1/L2](https://doi.org/10.3847/2041-8205/832/1/L2)
- Safarzadeh, M., Hamers, A. S., Loeb, A., & Berger, E. 2020, *ApJL*, 888, L3, doi: [10.3847/2041-8213/ab5dc8](https://doi.org/10.3847/2041-8213/ab5dc8)
- Samsing, J. 2018, *PhRvD*, 97, 103014, doi: [10.1103/PhysRevD.97.103014](https://doi.org/10.1103/PhysRevD.97.103014)
- Samsing, J., Askar, A., & Giersz, M. 2018a, *ApJ*, 855, 124, doi: [10.3847/1538-4357/aaab52](https://doi.org/10.3847/1538-4357/aaab52)
- Samsing, J., & D’Orazio, D. J. 2018, *MNRAS*, doi: [10.1093/mnras/sty2334](https://doi.org/10.1093/mnras/sty2334)

- Samsing, J., D’Orazio, D. J., Kremer, K., Rodriguez, C. L., & Askar, A. 2019a, arXiv e-prints, arXiv:1907.11231. <https://arxiv.org/abs/1907.11231>
- Samsing, J., Hamers, A. S., & Tyles, J. G. 2019b, *PhRvD*, 100, 043010, doi: [10.1103/PhysRevD.100.043010](https://doi.org/10.1103/PhysRevD.100.043010)
- Samsing, J., & Ilan, T. 2018, *MNRAS*, 476, 1548, doi: [10.1093/mnras/sty197](https://doi.org/10.1093/mnras/sty197)
- . 2019, *MNRAS*, 482, 30, doi: [10.1093/mnras/sty2249](https://doi.org/10.1093/mnras/sty2249)
- Samsing, J., MacLeod, M., & Ramirez-Ruiz, E. 2014, *ApJ*, 784, 71, doi: [10.1088/0004-637X/784/1/71](https://doi.org/10.1088/0004-637X/784/1/71)
- . 2018b, *ApJ*, 853, 140, doi: [10.3847/1538-4357/aaa715](https://doi.org/10.3847/1538-4357/aaa715)
- Samsing, J., & Ramirez-Ruiz, E. 2017, *ApJL*, 840, L14, doi: [10.3847/2041-8213/aa6f0b](https://doi.org/10.3847/2041-8213/aa6f0b)
- Samsing, J., Venumadhav, T., Dai, L., et al. 2019c, *PhRvD*, 100, 043009, doi: [10.1103/PhysRevD.100.043009](https://doi.org/10.1103/PhysRevD.100.043009)
- Sasaki, M., Suyama, T., Tanaka, T., & Yokoyama, S. 2016, *Physical Review Letters*, 117, 061101, doi: [10.1103/PhysRevLett.117.061101](https://doi.org/10.1103/PhysRevLett.117.061101)
- Schröder, S. L., Batta, A., & Ramirez-Ruiz, E. 2018, *ApJL*, 862, L3, doi: [10.3847/2041-8213/aacf8d](https://doi.org/10.3847/2041-8213/aacf8d)
- Sigurdsson, S., & Phinney, E. S. 1993, *ApJ*, 415, 631
- Silsbee, K., & Tremaine, S. 2017, *ApJ*, 836, 39, doi: [10.3847/1538-4357/aa5729](https://doi.org/10.3847/1538-4357/aa5729)
- Stephan, A. P., Naoz, S., Ghez, A. M., et al. 2016, *MNRAS*, 460, 3494, doi: [10.1093/mnras/stw1220](https://doi.org/10.1093/mnras/stw1220)
- Stone, N. C., & Leigh, N. W. C. 2019, *Nature*, 576, 406, doi: [10.1038/s41586-019-1833-8](https://doi.org/10.1038/s41586-019-1833-8)
- Stone, N. C., Metzger, B. D., & Haiman, Z. 2017, *MNRAS*, 464, 946, doi: [10.1093/mnras/stw2260](https://doi.org/10.1093/mnras/stw2260)
- Tagawa, H., Haiman, Z., & Kocsis, B. 2019, arXiv e-prints, arXiv:1912.08218. <https://arxiv.org/abs/1912.08218>
- Tanikawa, A. 2013, *MNRAS*, 435, 1358, doi: [10.1093/mnras/stt1380](https://doi.org/10.1093/mnras/stt1380)
- Toonen, S., Hamers, A., & Portegies Zwart, S. 2016, *Computational Astrophysics and Cosmology*, 3, 6, doi: [10.1186/s40668-016-0019-0](https://doi.org/10.1186/s40668-016-0019-0)
- VanLandingham, J. H., Miller, M. C., Hamilton, D. P., & Richardson, D. C. 2016, *ApJ*, 828, 77, doi: [10.3847/0004-637X/828/2/77](https://doi.org/10.3847/0004-637X/828/2/77)
- Venumadhav, T., Zackay, B., Roulet, J., Dai, L., & Zaldarriaga, M. 2019, arXiv e-prints, arXiv:1904.07214. <https://arxiv.org/abs/1904.07214>
- Woosley, S. E. 2016, *ApJL*, 824, L10, doi: [10.3847/2041-8205/824/1/L10](https://doi.org/10.3847/2041-8205/824/1/L10)
- . 2017, *ApJ*, 836, 244, doi: [10.3847/1538-4357/836/2/244](https://doi.org/10.3847/1538-4357/836/2/244)
- Yang, Y., Bartos, I., Gayathri, V., et al. 2019, *PhRvL*, 123, 181101, doi: [10.1103/PhysRevLett.123.181101](https://doi.org/10.1103/PhysRevLett.123.181101)
- Ye, C. S., Fong, W.-f., Kremer, K., et al. 2020, *ApJL*, 888, L10, doi: [10.3847/2041-8213/ab5dc5](https://doi.org/10.3847/2041-8213/ab5dc5)
- Zackay, B., Venumadhav, T., Dai, L., Roulet, J., & Zaldarriaga, M. 2019, arXiv e-prints, arXiv:1902.10331. <https://arxiv.org/abs/1902.10331>
- Zaldarriaga, M., Kushnir, D., & Kollmeier, J. A. 2018, *MNRAS*, 473, 4174, doi: [10.1093/mnras/stx2577](https://doi.org/10.1093/mnras/stx2577)
- Zevin, M., Pankow, C., Rodriguez, C. L., et al. 2017, *ApJ*, 846, 82, doi: [10.3847/1538-4357/aa8408](https://doi.org/10.3847/1538-4357/aa8408)
- Zevin, M., Samsing, J., Rodriguez, C., Haster, C.-J., & Ramirez-Ruiz, E. 2019, *ApJ*, 871, 91, doi: [10.3847/1538-4357/aaf6ec](https://doi.org/10.3847/1538-4357/aaf6ec)